

Single-cell landscape of functionally cured chronic hepatitis B patients reveals activation of innate and altered CD4-CTL-driven adaptive immunity

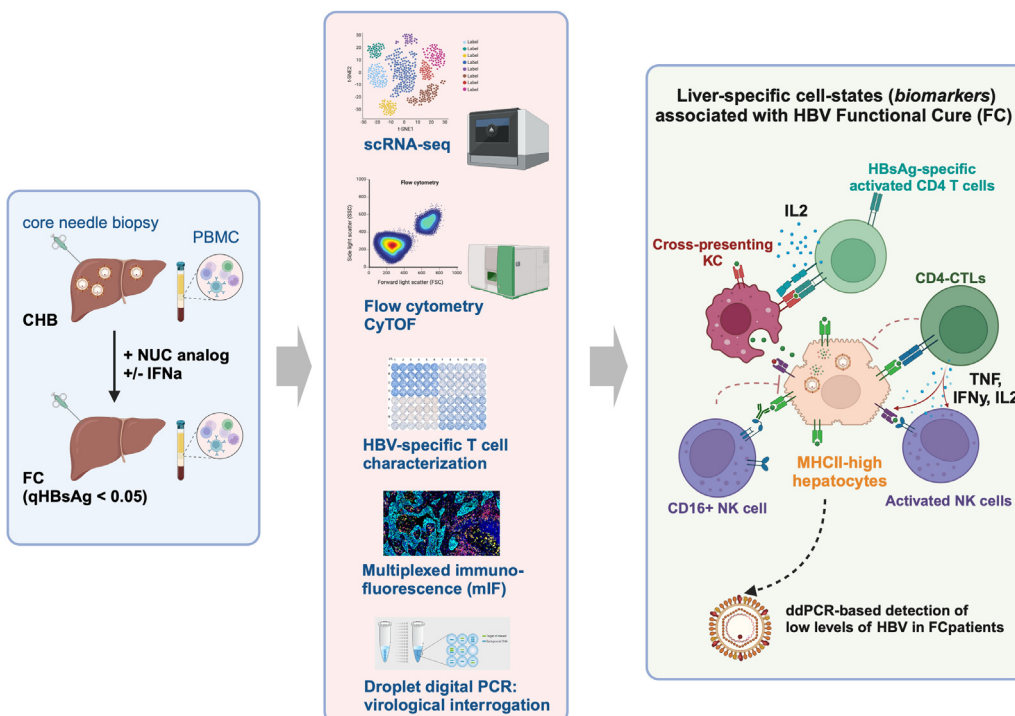
Authors

Balakrishnan Chakrapani Narmada, Atefah Khakpoor, Niranjan Shirgaonkar, ..., Massimo Levrero, Seng Gee Lim, Ramanuj DasGupta

Correspondence

mdclimsg@nus.edu.sg (S.G. Lim), dasguptar@gis.a-star.edu.sg (R. DasGupta).

Graphical abstract



Highlights

- An altered adaptive immune response – associated with CD4 cytotoxic T lymphocytes – emerges in functionally cured patients.
- Increased recruitment and margination of neutrophils in the liver suggests a low grade immune active state linked to functional cure.
- MHC class II-expressing hepatocytes were identified as accessory antigen-presenting cells.
- Alterations in the immuno-pathological cell states identified in the liver environment are not always reflected in peripheral circulation.

Impact and Implications

This study dissects the immuno-pathological cell states associated with functionally cured chronic hepatitis B (defined by the loss of HBV surface antigen or HBsAg). We identified the sustained presence of very low viral load, accessory antigen-presenting hepatocytes, adaptive-memory-like natural killer cells, and the emergence of helper CD4 T cells with cytotoxic or effector-like signatures associated with functional cure, suggesting previously unsuspected alterations in the adaptive immune response, as well as a key role for the innate immune response in achieving or maintaining functional cure. Overall, the insights generated from this study may provide new avenues for the development of alternative therapies as well as patient surveillance for better clinical management of chronic hepatitis B.

Single-cell landscape of functionally cured chronic hepatitis B patients reveals activation of innate and altered CD4-CTL-driven adaptive immunity

Balakrishnan Chakrapani Narmada^{1,2,†}, Atefah Khakpoor^{3,†}, Niranjan Shirgaonkar^{1,†}, Sriram Narayanan⁴, Pauline Poh Kim Aw¹, Malay Singh⁵, Kok Haur Ong⁵, Collins Oduor Owino^{1,6}, Jane Wei Ting Ng³, Hui Chuing Yew³, Nu Soibah Binte Mohamed Nasir³, Veonice Bijin Au⁴, Reina Sng⁴, Nivashini Kaliaperumal⁴, Htet Htet Toe Wai Khine³, Francesca Casuscelli di Tocco⁷, Otsuka Masayuki⁸, Shamita Naikar⁸, Hui Xin Ng³, Su Li Chia³, Cindy Xin Yi Seah⁹, Myra H.J. Alnawaz⁹, Chris Lee Yoon Wai³, Amy Yuh Ling Tay³, Kamarjit Singh Mangat³, Valerie Chew⁸, Weimiao Yu^{4,5}, John Edward Connolly^{4,6,10,11}, Giridharan Periyasamy², Marie-Laure Plissonnier⁷, Massimo Leviero^{7,12,13,14}, Seng Gee Lim^{4,9,15,*}, Ramanuj DasGupta^{1,*}

Journal of Hepatology 2024. vol. 81 | 42–61



See Editorial, pages 14–16

Background & Aims: Hepatitis B surface antigen (HBsAg) loss or functional cure (FC) is considered the optimal therapeutic outcome for patients with chronic hepatitis B (CHB). However, the immune-pathological biomarkers and underlying mechanisms of FC remain unclear. In this study we comprehensively interrogate disease-associated cell states identified within intrahepatic tissue and matched PBMCs (peripheral blood mononuclear cells) from patients with CHB or after FC, at the resolution of single cells, to provide novel insights into putative mechanisms underlying FC.

Methods: We combined single-cell transcriptomics (single-cell RNA sequencing) with multiparametric flow cytometry-based immune phenotyping, and multiplexed immunofluorescence to elucidate the immunopathological cell states associated with CHB vs. FC.

Results: We found that the intrahepatic environment in CHB and FC displays specific cell identities and molecular signatures that are distinct from those found in matched PBMCs. FC is associated with the emergence of an altered adaptive immune response marked by CD4 cytotoxic T lymphocytes, and an activated innate response represented by liver-resident natural killer cells, specific Kupffer cell subtypes and marginated neutrophils. Surprisingly, we found MHC class II-expressing hepatocytes in patients achieving FC, as well as low but persistent levels of covalently closed circular DNA and pregenomic RNA, which may play an important role in FC.

Conclusions: Our study provides conceptually novel insights into the immuno-pathological control of HBV cure, and opens exciting new avenues for clinical management, biomarker discovery and therapeutic development. We believe that the discoveries from this study, as it relates to the activation of an innate and altered immune response that may facilitate sustained, low-grade inflammation, may have broader implications in the resolution of chronic viral hepatitis.

© 2024 The Authors. Published by Elsevier B.V. on behalf of European Association for the Study of the Liver. This is an open access article under the CC BY-NC-ND license (<http://creativecommons.org/licenses/by-nc-nd/4.0/>).

Introduction

Chronic HBV infection (CHB) affects more than 257 million people, mainly in the Asia-Pacific and African regions, leading to an estimated 800,000 deaths annually from cirrhosis and hepatocellular carcinoma.¹ Currently available antiviral therapies suppress viral replication but fail to eliminate infection due to the persistent pool of covalently closed circular DNA (cccDNA) in hepatocytes.^{2,3} Due to existing challenges in achieving complete cure and the clearance of viral infection in patients with CHB, it is the loss of viral surface antigen (HBsAg) with or without

appearance of anti-HBs antibodies in patient serum, also known as functional cure (FC), that is accepted as the desired therapeutic endpoint in the clinic.⁴ The clearance of viral infection is largely dependent on a robust and long-lasting adaptive immune response. Virus-specific CD8 T cells are known to be involved in the resolution of acute HBV infection.^{5,6} However, in patients with CHB, HBV-specific CD8 T cells are terminally exhausted due to chronic stimulation by high levels of HBV antigens.⁷ Recent studies have shown that impairment of adaptive immune responses is also a function of the duration of exposure to

Keywords: liver; single cell RNA-seq; HBsAg; viral hepatitis; HBV; CD4-CTL; immune; accessory APC; neutrophils.

Received 29 December 2022; received in revised form 5 February 2024; accepted 15 February 2024; available online 28 February 2024

* Corresponding authors. Addresses: Institute of Molecular and Cell Biology, A*STAR, 61 Biopolis Drive, Proteos, Singapore, 138673, Singapore (S.G. Lim), or Laboratory of Precision Medicine and Cancer Evolution, Genome Institute of Singapore, Agency for Science, Technology and Research (A*STAR), 60 Biopolis St., #02-01 Genome, Singapore 138672; Tel.: +65 6808 8005 (R. DasGupta).

E-mail addresses: mdclimsg@nus.edu.sg (S.G. Lim), dasguptar@gis.a-star.edu.sg (R. DasGupta).

† Equal contribution

<https://doi.org/10.1016/j.jhep.2024.02.017>



ELSEVIER

Journal of Hepatology, July 2024. vol. 81 | 42–61



viral antigens in addition to high antigen load.^{1,6,8} The specific function of the innate immune response in CHB remains debatable and relatively poorly understood. The innate immune response is generally thought to be functionally impaired in CHB.^{9–11} However, a recent study using a mouse model of HBV infection identified a specific Kupffer cell (KC) population (constituting resident, embryonically-seeded macrophages in the liver) that was shown to reinvigorate the anti-viral function of HBV-specific CD8 T cells in the presence of IL2.¹² Additionally, other recent studies have revealed a positive correlation between increased cytotoxic activity of natural killer (NK) cells and liver inflammation, typically in patients who clear HBsAg upon cessation of nucleoside analogue (NUC) treatment.¹² These studies allude to a potential function for innate immune cells in the resolution of CHB.^{11–13} Even though recent studies have explored the dynamics of the liver environment in different phases of CHB using multiplexed imaging and bulk RNA sequencing^{14,15} in biopsies, and fine-needle aspirate-based single-cell RNA sequencing (scRNA-seq),¹⁶ disease-associated cell states (DACS) in FC patients have not been interrogated. Thus, there is a clear unmet need for a comprehensive, high-resolution investigation of key cell types or cell states and regulatory cell-cell interactions that may modulate underlying mechanisms involved in maintenance of FC.

In this study, we sought to explore the mechanistic basis for sustained control of HBsAg loss. Importantly, through the systematic analyses of transcriptomic profiles, inferred cell-cell interactions, and flow cytometry-based validation studies, we present a comprehensive, comparative atlas that represents the single cell landscape of intra-hepatic environment and matched peripheral blood mononuclear cells (PBMCs) of patients with CHB, including non-responders vs. those achieving FC.

Materials and methods

Study approval

Peripheral blood and biopsy sampling as well as clinical assessment were performed at the National University Hospital (Singapore) in accordance with the Declaration of Helsinki. Written informed consent was obtained. The study was reviewed and approved by Singapore National Health Group Domain Specific Review Board (DSRB reference number 2000/00828).

Patients

Paired blood and biopsy of 29 patients with CHB (across different phases based on EASL guidelines)^{4,17} and 9 patients who achieved FC (duration of HBsAg loss at the time of biopsy range from 7 to 84 months [median = 42 ± 30.1 months], quantitative HBsAg [qHBsAg] <0.05 IU/ml) were obtained for this study. Specific details of samples processed by scRNA-seq and Flow Cytometry are available at Table 1. Two needle core biopsies and were obtained from each patient with signed consent using the biopince liver biopsy instrument which were used for scRNA-seq and, multi-parametric Flow cytometry analysis along with matched PBMCs at the same timepoint. Table 1 also summarizes the clinical and virological parameters of all patients.

Clinical and virological parameters

HBV DNA levels were measured in all patients (COBAS AmpliPrep/COBAS TaqMan HBV test v2.0; Roche Molecular Diagnostics) and viral parameters (qHBsAg, HBeAg, and anti-HBe levels) were assessed with Roche COBAS 8000 (e801) system using Electrochemiluminescence Immunoassay (ECLIA) method, and HBV genotype was recorded where available. All patients included were HCV, HDV and HIV negative.

Single-cell dissociation for scRNA-Seq

One liver biopsy core and matched PBMC were collected from patients with institutional ethics approval as described earlier. Liver biopsies were processed based on an enzymatic dissociation protocol adapted from Sharma *et al.* 2020.¹⁸ Briefly, biopsies were stored and transported in HypoThermosol® FRS Preservation Solution (Sigma H4416-100 ml) solution at 4 °C until further processing. The tissue sample was first minced to 2-3 mm pieces using sterile scalpels. Collagenase P solution (from Roche (11249002001) 2 mg/ml in DMEM) was added to the tissue and the tissue was kept in a 37 °C shaking incubator to allow single cell dissociation for 10-15min. Cell suspension was washed with PBS (no Mg²⁺ or Ca²⁺) with 1% w/v BSA, and 1 mM EDTA solution filtered through 70 µm cell strainer to remove cell debris. The cells were then centrifuged at differential speeds to collect parenchymal fraction (100xg) and non-parenchymal fractions (400xg). If red blood cells were seen in the pellet, RBC lysis was performed using 10x RBC lysis buffer (Biologend 420301) for 5min before proceeding to the next wash. Filtered through 40 µm filter and washed with PBS (no Mg²⁺ or Ca²⁺) with 1% w/v BSA solution. Cell count and viability of the dissociated cells were evaluated by Trypan Blue staining before combining the parenchymal and non-parenchymal fractions in a 1:1 ratio to make up 30 µl of 1000cells/µl processing for 10x 3' scRNA-seq v3 preparation.

Flow cytometry sample preparation

For T cell and NK cell deep phenotyping by multiparametric Flow Cytometry, 23 patients (indicated in Table 1) were used and the rest were excluded due to non-availability of material or low viability of cells. To isolate the leukocytes, one liver biopsy core was subjected to mechanical disruption and filtration through a 70 µm cell strainer (BD biosciences). Removal of the parenchymal cells and isolation of lymphocytes were done through centrifugation at 50xg without brake. Isolated lymphocytes were washed, counted to evaluate the cell viability and used immediately after isolation for further flow cytometry related analysis (see Tables S1 and S2 for list of antibodies used).

Matched PBMC isolation from heparinized blood was carried out by density centrifugation with Ficoll-Hyperaque Plus (GE Healthcare). Isolated PBMCs were cryopreserved in 10% dimethyl sulfoxide (DMSO) (Sigma Aldrich) prior to further use.¹⁹

Single-cell RNA-seq sample preparation, cDNA & library generation, sequencing

An aliquot of the prepared single cells was counted, and cell concentration was adjusted to 800 cells/µl. GEM generation and 3' mRNA-seq gene expression libraries were prepared using the Chromium Next GEM Single Cell 3' GEM, Library and

Table 1. Clinical and virological parameters of all patient samples based on EASL guidelines, and methods for profiling (single-cell RNA-seq and flow cytometry).

Type	ID	EASL classification	Sex	Age	ALT (IU/ml)	AST (IU/ml)	HBV DNA (IU/ml)	HBeAg	qHBsAg (IU/ml)	Anti-HBs Ab (IU/L)	Months of HBsAg clearance	Genotype	Overall treatment category	Flow_PBMC	Flow_Biopsy	ScBiopsy	ScPBMC
NonSloss	CHB1	Phase 2	M	30	108	43	131,309,541	Positive	108,706.77	Non-reactive	NA	B	Naïve	Yes	Yes	No	No
NonSloss	CHB2	Phase 2	F	54	86	55	894,000,000	Positive	52,385	NA	NA	C	Naïve	Yes	Yes	Yes	Yes
NonSloss	CHB3	Phase 2	F	48	70	55	19,500,000	Positive	29,505.43	NA	NA	B	Naïve	Yes	Yes	Yes	Yes
NonSloss	CHB4	Phase 2	M	55	41	43	756,000,000	Positive	13,877.52	NA	NA	C	Naïve	Yes	Yes	Yes	Yes
NonSloss	CHB5	Phase 2	F	37	41	42	406,000,000	Positive	130,880	Non-reactive	NA	A	Naïve	Yes	Yes	Yes	Yes
NonSloss	CHB8	Phase 2	F	33	77	45	83,000,000	Positive	3,505.43	Non-reactive	NA	C	Naïve	Yes	Yes	Yes	Yes
NonSloss	CHB10	Phase 2	M	35	86	43	3,130,000	Positive	2,746.81	Non-reactive	NA	C	Naïve	Yes	Yes	No	Yes
NonSloss	CHB23	Phase 2	F	33	192	84	73,565,512	Positive	10,677.82	Non-reactive	NA	B	Naïve	No	No	Yes	Yes
NonSloss	CHB24	Phase 2	F	39	43	35	622,663,241	Positive	328,576	Non-reactive	NA	B	Naïve	No	No	Yes	Yes
NonSloss	CHB28	Phase 2	M	32	169	67	134,685,627	Positive	27,752.05	Non-reactive	NA	C	Naïve	No	No	Yes	Yes
NonSloss	CHB31	Phase 2	F	56	175	206	1,590,000	Positive	67.92	Non-reactive	NA	C	IFN + NUC	No	No	Yes	Yes
NonSloss	CHB12	Phase 3	M	52	73	76	0	Negative	28.02	Non-reactive	NA	C	NUC only	Yes	Yes	No	No
NonSloss	CHB13	Phase 3	F	70	63	49	0	Negative	1.91	Non-reactive	NA	B	IFN + NUC	Yes	Yes	Yes	Yes
NonSloss	CHB15	Phase 3	F	62	79	47	39	Negative	2.03	Non-reactive	NA	ND	Naïve	Yes	Yes	No	Yes
NonSloss	CHB16	Phase 3	M	33	19	18	1,342	Negative	753.7	Non-reactive	NA	B	Naïve	No	Yes	No	No
NonSloss	CHB17	Phase 3	M	54	14	24	0	Negative	0.14	Non-reactive	NA	C	IFN + NUC	Yes	Yes	No	No
NonSloss	CHB20	Phase 3	M	72	26	23	0	Negative	81.61	Non-reactive	NA	B	NUC only	Yes	Yes	Yes	Yes
NonSloss	CHB30	Phase 3	M	61	42	38	0	Negative	9.02	Non-reactive	NA	ND	NUC only	No	No	Yes	Yes
NonSloss	CHB32	Phase 3	M	64	24	26	0	Negative	55.19	Non-reactive	NA	C	IFN + NUC	No	No	No	Yes
NonSloss	CHB6	Phase 4	M	47	118	57	4,385,858	Negative	3,747.64	Non-reactive	NA	B	Naïve	Yes	Yes	No	No
NonSloss	CHB7	Phase 4	M	48	50	37	4,520	Negative	1,177.48	Non-reactive	NA	B	Naïve	Yes	Yes	Yes	Yes
NonSloss	CHB9	Phase 4	F	59	22	30	21,023	Negative	2,557.7	Non-reactive	NA	C	Naïve	Yes	Yes	Yes	Yes
NonSloss	CHB11	Phase 4	F	41	13	15	10,200	Negative	7,056	Non-reactive	NA	B	Naïve	Yes	Yes	No	Yes
NonSloss	CHB14	Phase 4	M	51	88	37	81,401	Negative	742.06	Non-reactive	NA	C	Naïve	Yes	Yes	Yes	Yes
Sloss	FC1	FC	M	50	17	23	0	Positive	<0.05	1	8	C	IFN + NUC	Yes	Yes	Yes	Yes
Sloss	FC2	FC	M	49	24	22	20	Negative	<0.05	2.53	7	C	IFN + NUC	Yes	Yes	Yes	Yes
Sloss	FC3	FC	M	65	13	25	0	Negative	<0.05	486	24	B	IFN only	Yes	Yes	Yes	Yes
Sloss	FC4	FC	F	53	19	21	0	Negative	<0.05	329	72	C	IFN + NUC	Yes	Yes	Yes	Yes
Sloss	FC5	FC	M	57	40	36	0	Negative	<0.05	3	60	ND	IFN + NUC	Yes	Yes	Yes	Yes
Sloss	FC6	FC	M	44	35	22	0	Negative	<0.05	35	84	C	IFN + NUC	Yes	Yes	Yes	Yes
Sloss	FC7	FC	M	67	18	15	0	Negative	<0.05	0	24	ND	Naïve	No	Yes	No	No
Sloss	FC8	FC	F	62	18	23	0	Negative	<0.05	2	72	ND	IFN + NUC	Yes	No	Yes	Yes
Sloss	FC9	FC	M	45	68	41	0	Negative	<0.05	6	24	C	IFN + NUC	Yes	No	Yes	Yes

ALT, alanine aminotransferase; AST, aspartate aminotransferase; CHB, chronic hepatitis B; FC, functional cure; HBsAg, HBV surface antigen; IFN, interferon; NonSloss, no HBsAg loss; NUC, nucleos(t)ide analogues; PBMC, peripheral blood mononuclear cells; Sloss, HBsAg loss. Note: patients with CHB are stratified based on EASL guidelines as well as qHBsAg level (IU/ml) (>10,000, 1,000–10,000, 0.05–1,000) and FC.

Gel Bead Kit v3.1 (10x Genomics) according to the manufacturer's guidelines. Briefly, 16.5 µl of cells were added into the master mix for a targeted cell recovery of 8000 cells. This was then loaded into a single-cell chip which was then inserted into the 10x Genomic Chromium controller for GEM generation. Once the run was completed, the samples were carefully transferred into clean tubes for reverse transcription. The samples were then purified using Dynabeads followed by 12 cycles of cDNA amplification. After that, samples were purified using SPRI-select reagent before profiling them on the Bioanalyzer (Agilent) and genomic scRNA libraries were constructed. This consisted of a series of steps involving fragmentation, end repair, A-tailing, adaptor ligation and a final amplification of 14 cycles. Finally, using SPRIselect reagent, the samples were purified and the required size of 300–700 bp was selected. Quantification and quality check was done using Bioanalyser (Agilent). Each of the samples XHL102 to XHL135 were sequenced in-house on a single lane on HiSeq 4000, whereas samples XHL232 to XHL343 were pooled with maximum of 8 samples in each lane and sequenced on NovaSeq S4 (Novogene). Both platforms generated paired-end reads with a read length of 151 bp.

Single-cell RNA-seq analysis

Single-cell datasets generated in-house from CHB and FC patient livers and PBMC samples were processed using the Cellranger 6.0.1 pipeline and were mapped to the human reference genome (GrCh38). The output, raw feature-barcode matrix, was then imported into ScanPy (v1.7.1). Cells of low quality (cells with less than 200 genes per cell) and cells expressing rare genes (genes expressed by less than 30 cells) were then removed from the matrix. For the scRNA-seq data, out of 31 total samples profiled, 8 samples from the liver and 4 samples from the PBMC were removed due to poor sample quality based on the read count and the number of reads mapped to the human transcriptome. Cells with a mitochondrial percentage greater than 20% or cells with the number of detected genes less than 200 were excluded from the matrix. An upper limit of 6,000 genes was used and the putative cell doublets were removed using the Scrublet package.²⁰ The cell counts were then normalized using `scipy.pp.normalize_per_cell` with a scaling factor of 10,000 and gene expression was scaled to unit variance and a mean value of 0 using `scipy.pp.scale`. Dimensionality reduction of the data was done with principal component analysis using the `scipy.tl.pca` function and the `scipy.pl.pca_variance_ratio` plot was used to determine the inflection point after which no remarkable change in the variance was observed. The neighborhood graph for clustering was calculated using `scipy.pp.neighbors` while the `scipy.tl.leiden` function was used to cluster the cells using Leiden clustering. Batch effects were observed after clustering which could be attributed to the samples being sequenced using two different platforms, NovaSeq and Illumina HiSeq 4000. The batch correction pipeline, Harmony was used to integrate the samples together. All steps starting from dimensionality reduction were repeated until well-defined leiden clusters were obtained. Differentially expressed genes across the leiden clusters were determined using `scipy.tl.rank_genes_groups` and were used to check cluster validity. Cell subtypes were then assigned to these clusters using annotation

pipelines like singleR and Azimuth.²¹ Manual annotation using well-known cell type markers from available literature were also employed for confirmation. Each individual cell subtype was segregated and undesirable sources of variations like variable library sizes, mitochondrial genes, cell cycle genes were regressed out using the `scipy.pp.regress_out` function. Cell subtype were then re-clustered and the resulting leiden clusters specific to each cell type were analyzed between CHB and FC patients using a battery of pipelines like CellPhoneDB²² for cell-cell communication analysis, and RNA Velocity²³ for specific cell type trajectory analysis.

We performed Harmony-based integration of healthy liver scRNA-seq data from MacParland *et al.*²⁴ with our scRNA-seq data from CHB and FC patients.

Pathway analysis

Differentially expressed genes between clusters or between the two conditions (CHB and FC) were determined through Wilcoxon statistical tests (*p* value<0.01). Upregulated pathway analysis of these differentially expressed genes was performed using open-source application Metascape²⁵ and visualized through the ggplot2 function in R.

Direct ex vivo flow cytometry analysis

Freshly isolated leukocytes from liver biopsies and thawed PBMCs were stained with Live/Dead cell viability stain (Invitrogen, California, USA) followed by surface staining for 30 minutes on ice. All antibodies used for direct ex vivo analysis of NK and T cells are summarized in Tables S1 and S2. Cells were acquired on BD FACSymphony™ A5 (BD Biosciences) cell analyzer for NK and T cell analysis. Data was analysed using FlowJo version 10 (BD Biosciences). Heatmaps were generated using Heatmapper.²⁶

HBV peptide libraries

HBV-specific T cells were identified using libraries of 313 fifteen-mer peptides overlapping by 10 amino acids^{7,19} covering the whole proteome of HBV genotypes B and C (GenBank AF121243 and AF112063). Purity of the peptides was 80% and their composition was confirmed by mass spectrometry. The peptides were purchased from Mimotopes and were pooled as described previously.¹⁹

T-cell culture

For *in vitro* assays, T cell lines were generated as mentioned before^{7,19} using thawed matched PBMCs. Briefly, 20% of the PBMCs were pulsed with 10 µg/ml of the overlapping HBV peptides for 1 hour at 37 °C followed by washing. Subsequently peptide-pulsed cells were co-cultured with remainder of the cells in AIM-V supplemented with 2% AB human serum (Gibco; Thermo Fisher Scientific). *In vitro* generated T cell lines were kept in culture for 10 days in the presence of 20 U/ml of recombinant IL2 (Miltenyi Biotech).^{7,19}

ELISpot

ELISpot assay for detection of IFNγ producing cells was done on the *in vitro* expanded T cell lines using the HBV peptide libraries pooled into mixtures as following: X, Core, Envelope 1

and 2, HBV pol 1,2,3 and 4. T cell lines were incubated overnight at 37 °C with HBV peptide pools (5 µg/ml per peptide). The final concentration of DMSO did not exceed 0.5%. IFNγ ELISpot (Mabtech) was done as described previously.¹⁹

Intracellular cytokine staining

In vitro-expanded T cells were incubated with HBV pool peptides overnight at 37 °C (5 µg/ml) in the presence of 2 µg/ml Brefeldin A (Sigma-Aldrich). Cells were cultured with stimulation cocktail (Thermo Fisher Scientific) as positive control. Cells were stained with Live/Dead fixable Texas red stain kit (ThermoFisher Scientific) followed by surface staining with CD8-PE (BD Biosciences) and CD4-BB515 (BD Biosciences). Cells were then fixed and permeabilized using Cytofix/Cytoperm kit (BD Pharmingen) and stained with IFNγ-Percp and TNFα-APC-Cy7(Biolegend Technologies). Cells were acquired on an LSR Fortessa cytometer (BD Biosciences) and analyzed using FlowJo version 10 (BD Biosciences).

Cytokine-chemokine analysis – Luminex

Three multiplex panels: Immune Monitoring 65-plex ProcartaPlex Panel (Thermofisher, Waltham, Massachusetts, USA), Human Soluble Cytokine Receptor Panel and Human Liver Protein Panel (Merck Millipore, Billerica, MA, USA) were used to measure cytokines, chemokines and soluble factors in patient plasma samples. Assays were performed as per manufacturer's instructions. Plates were washed using Tecan Hydrospeed Washer (Tecan, Männedorf, Switzerland) and read with Flexmap 3D system (Luminex Corp, Austin, TX, USA). Data analysis was done using the Bio-Plex manager 6.2 software with a 5-parameter curve-fitting algorithm applied for standard curve calculations. A percentage-based proportionality bar chart was created using the derived cytokines levels to make them comparable to each other.

Cytometry by time-of-flight

Cytometry by time-of-flight staining was performed as previously described²⁷ with a panel of 39 antibodies (Table S3) and analysed using a Helios mass cytometer (Fluidigm, USA). Data were downsampled to 10,000 viable CD45+ cells for in-house developed extended poly-dimensional immunome characterisation.²⁸ Clustering was performed with the FlowSOM algorithm, dimension reduction by tSNE, and visualisation with the R shiny app 'SciAtlasMiner'. Enriched clusters were identified by two-tailed Mann-Whitney *U* test and validated with manual gating using FlowJo (V.10.5.2; FlowJo, USA).

Quantification of cccDNA, DNA and 3.5 kb RNA in liver samples with ddPCR

All extractions were performed using the Allprep DNA/RNA Qiagen kit according to the manufacturers' specifications (Qiagen, Hilden, Germany). Liver samples were homogenized on ice in RLT Buffer using a TissueRuptor (Qiagen, Hilden, Germany). The quantity and integrity of the extracted DNA and RNA were assessed using a NanoDrop Spectrophotometer (NanoDrop Technologies, Wilmington, USA). Prior to cccDNA amplification, DNA was treated with 10U of Plasmid-safe DNase (Epicentre® by Illumina, Madison, USA) to digest any residual HBV replicative intermediates or genomic DNA in the

samples. The quantification of the absolute copy numbers of intrahepatic cccDNA, DNA and 3.5 kb RNA (pregenomic RNA) was performed using the QX100TM Droplet Digital TM PCR System (Bio-Rad, Hercules, USA) according to the manufacturer's instructions with primers and fluorescence dual hybridization probes specific for cccDNA, total HBV DNA and 3.5 kb RNA (Table S4). Briefly, for the cccDNA/DNA quantification, the 22 µl digital droplet PCR (ddPCR) reactions comprised 2X ddPCR Supermix for probes (Bio-Rad, Hercules, USA), 900 nM primers, 250 nM probe, and 100 ng of sample. PCR amplification was performed in the C1000 Touch™ Thermal cycler (Bio-Rad) with a ramp rate of 2 °C/s and the lid heated to 105 °C, according to Bio-Rad recommendations. PCR comprised 40 cycles of denaturation at 95 °C for 30 s and 60 °C for 1min. Final enzyme inactivation was performed for 10 minutes at 98 °C and the reaction was kept at 4 °C. For the 3.5 kb RNA quantification, the 22 µl One-step RT-ddPCR Advanced reaction mixtures (Bio-Rad, Hercules, USA) were comprised 2X ddPCR Supermix for probes, 20 U/µL of reverse transcriptase enzyme, 900 nM primers and 250 nM probe mix, 15 nM of DTT and 100 ng of sample. Reverse transcription step was performed at 50 °C followed by 95 °C inactivation for 10min. PCR amplification was performed in the C1000 Touch™ Thermal cycler (Bio-Rad) with a ramp rate of 2 °C/s and the lid heated to 105 °C, according to Bio-Rad recommendations. PCR comprised 40 cycles of denaturation at 95 °C for 30 s and 60 °C for 1 min. Final enzyme inactivation was performed for 10 minutes at 98 °C and the reaction was kept at 4 °C. Droplet formation was carried out using a QX200 Automated droplet generator with specific oil for probes (Bio-Rad, Hercules, USA) to partition the sample into about 20,000 droplets in 20 µL. After amplification, the plate was placed into the QX100 Droplet Reader (Bio-Rad, Hercules, USA). The ddPCR data were analysed using the QuantaSoft analysis software version 1.7.4 (Bio-Rad, Hercules, USA). To express the copies/cell, we quantified beta-globin (ThermoFisher Scientific, Waltham, MA, USA) in the same sample by ddPCR. Reactions with less than 5 positive droplets were considered negative. The limit of detection for cccDNA was 4.8 copies/10.6 cells (95% confidence interval: [3.3; 7]), calculated by Probit analysis on a sample composed of serial dilution of a minicircle HBV into genomic DNA.²⁹ cccDNA transcription activity was estimated as the ratio of 3.5 kb RNA/cccDNA. The analysis of HBV-negative liver biopsy samples served to confirm the specificity of the technique and as reference for the settings of thresholds discriminating positive from negative droplets.²⁹

Single-cell cDNA amplification using bait capture and viral mapping

Amplified single-cell cDNA samples following step 2 of the Chromium Single Cell 3'kit were used to create HBV bait-captured sequencing libraries. Libraries were built using the NEBNext Ultra II FS DNA Library Prep Kit followed by baiting and capturing using the IDT xGen hybridization capture of DNA libraries kit according to the manufacturers' instructions. Briefly, samples were fragmented, adaptor ligated, and amplified for 20 cycles. In-house designed biotinylated-labelled oligos or baits of 150bp in length which binds to HBV genome were used in this experiment. Baits and samples were hybridized at 65C for 16 hours before streptavidin beads were used to

capture the baited materials. This was followed by a series of heated and room temperature washes and finally a 20 cycles amplification step. The quality and quantity of the libraries were then assessed using the Tape Station (Agilent). Equimolar samples were pooled and sequenced on the Illumina HiSeqX with sequencing length of 2 x 151bp. ViPR pipeline (<https://github.com/CSB5/ViPR2>) was used to process and to analyse the sequencing fastq files. The coverage files were obtained as an output of the pipeline.

Multiplexed immunofluorescence, machine-based learning, and image analysis

Multiplexed image scanning of the tissue sections, stained with either the FixVUE T-act and FixVUE I/O myeloid-derived suppressor cell (MDSC) Kits (Ultivue), was performed on the Zeiss Axioscan.Z1 Imaging system Carl Zeiss Microscopy. All the WSI images were acquired at 0.325 μm per pixel resolution ($\times 20$ magnification). The multiplexed image processing pipeline developed by Singh *et al.* (manuscript under review; unpublished data) has been adapted for our analysis of multiplexed images. The MDSC stained tissue images were annotated for antigen-presenting cell (APC)-rich regions, Immune Infiltrate, and parenchymal regions. We used free-hand drawings over the tissue whole slide images to annotate these tissue types in A! HistoNotes software. The APC-rich region was defined based on high HLA-DR expression. Immune infiltrate region had both HLA-DR and CD3 expression. The parenchymal regions are regions excluding APC-rich or Immune infiltrate regions' criterions. The MDSC image annotations were then aligned to the corresponding T-act image for subsequent cellular level analysis. This image alignment was done using the DAPI channels in MDSC and T-act images. The image processing pipeline utilises mutual information between the DAPI channels in MDSC and T-act images for image registration. The registration algorithm does a multimodal registration to transform a given MDSC image to the T-act image. The final transformation was defined to be affine allowing only rotation and translation operations. There was no scaling or shearing operation. An evolutionary algorithm³⁰ was used to optimise the pixel intensity registration via *imregconfig* function in MATLAB (version 2021a).

The nuclei segmentation was done inside the detected tissue region by QuPath (version 0.2.0-m2)³¹ in the multiplexed immunofluorescence (mIF) images using DAPI channel. We used unimodal thresholding developed by Rosin *et al.*³² for the identification the positive cells, which uses the distribution of mean signal intensity within the full cell area to define an adaptive threshold at a given non-nuclei fluorescence channel. Eventually, the cellular phenotype for a given cell was defined using the corresponding positive status in various fluorescence channels. Cell density (#cells/mm²) was defined by counting the number of positive cells within a given tissue region, measured in mm². All the cell phenotypes in the both MDSC and T-act panels were quantified as cell density for each patient. Spatial phenotypes as defined by Singh *et al.* (manuscript under review; unpublished data) to quantify cell-cell interactions were also used. These spatial phenotypes quantified cellular neighbourhood densities (#cells/mm²) and pairwise cell-cell distances (μm). Pairwise cell distances were computed between the centroids of the corresponding cells. These spatial phenotypes use a radius of 130 μm wherein we used PanCK/

SOX10+ epithelial cells paired with the immune cells. We quantified the spatial phenotype via pairwise neighbourhood density (#cells/mm²), nearest neighbour distance (μm) and mean neighbourhood density (#cells/mm²). All the cell density and spatial phenotypes were statistically analysed for differences across patient grading and tissue type groups.

Statistical analysis

Statistical significance was determined by GraphPad Prism using methods stated in the figure legends. $p \leq 0.05$ was considered significant. Details of the statistical tests are provided in each of the legend for the main and the supplementary figures.

Results

Single-cell atlas of liver and matched PBMCs from CHB and FC

In this cross sectional study, patients were categorized as having CHB (either treated or treatment-naïve; $n = 29$) where viral HBsAg is detectable, or having achieved FC ($n = 9$). Functionally cured patients displayed clearance of viral HBsAg either upon treatment ($n = 7$) or spontaneously ($n = 2$) and were profiled between 7 to 84 months after the loss of HBsAg. Within this FC cohort, most patients displayed the sustained presence of anti-HBs antibodies (Fig. 1A and Table 1). Total cells isolated from core needle biopsies of liver and patient-matched PBMCs were subjected to scRNA-seq (15 CHB and 8 FC, after quality control) using the 10x Chromium platform, and multiparametric flow cytometry (17 CHB and 7 FC, after quality control). Wherever applicable, mIF staining, and image analysis was employed for validation studies on tissue sections generated from the same liver biopsies (see Fig. 1A for overall workflow). For focused phenotypic analysis of immune cell subsets and HBV-specific T cells, patients with CHB were stratified based on their qHBsAg levels, from high (>10,000 IU/ml), medium (1,000-10,000 IU/ml), and low (0.05-1,000 IU/ml), as described in Table 1 and compared with FC patients. Complete information on CHB disease phases based on EASL guidelines,^{4,17} viral parameters, patient age, and alanine aminotransferase levels are also provided in Table 1. Notably, our patient cohorts stratified mainly into HBeAg+-/- chronic hepatitis (Phase 2 and 4), and FC (HBsAg negative).

Distinct alterations in the composition of adaptive and innate immune cells observed in liver vs. matched PBMCs from FC patients

Single-cell transcriptomic profiling of CHB ($n = 15$) and FC ($n = 8$) patients captured 47,109 cells within the liver comprising 26 distinct major cell types/states, as determined by Leiden-based clustering, representing epithelial (hepatocytes, and cholangiocytes), immune (T cells, B cells, NK cells, monocytes, macrophages, dendritic cells, neutrophils, and mast cells), endothelial and stellate cells (Fig. 1B-B'). Similarly, profiling of matched PBMCs revealed a capture of 44,396 cells constituting 17 different immune cell subtypes, mainly comprising T, NK, monocytes, dendritic cells (DCs) and B cells (Fig. 1E-E'). We employed Harmony-based integration³³ to eliminate any variations arising from batch effects (Fig. S1A,B) and observed clear

Single cell atlas of functionally cured CHB patients

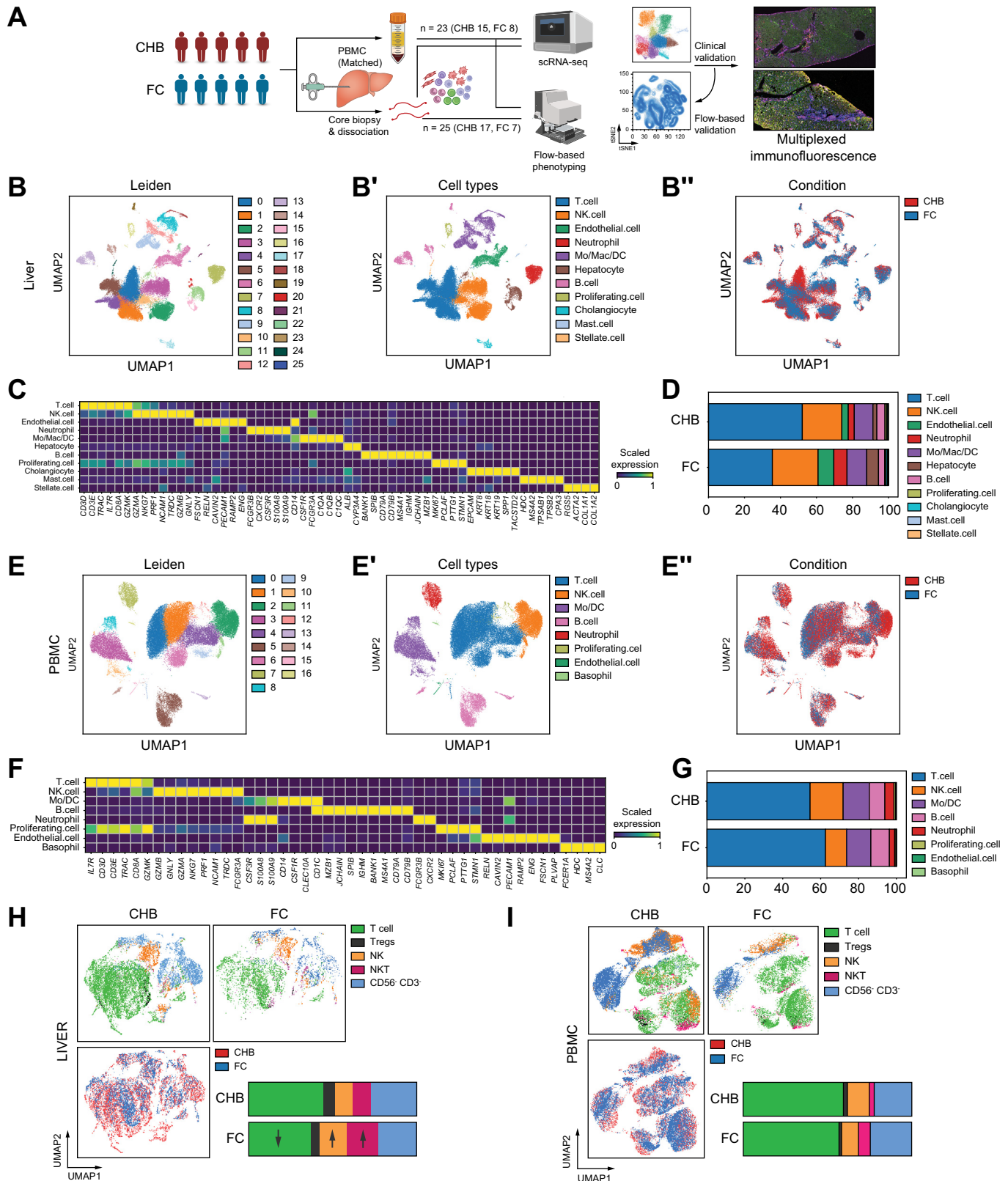


Fig. 1. Single-cell transcriptomic atlas of liver and matched PBMCs isolated from CHB vs. FC patients. (A) Schematic of overall workflow summarizing patient cohort, sample collection and experimental design. Matched PBMC and liver biopsy (2 cores) of CHB vs. FC subjected to scRNA-seq, multiparametric flowcytometry and multiplexed immuno-fluorescence. (B) UMAP projection of Leiden-based clustering of ~47,109 scRNA-seq libraries generated from the liver biopsies of CHB and FC patients identifies 26 distinct cell states. (B') Annotation of Leiden clusters based on the top DEGs and reference-based markers identifies 11 major cell types. (B'') Condition-wise annotation of scRNA-seq data from the two patient cohorts of CHB (red) vs. FC (blue) within the liver. (C) Heatmap of cell type-specific markers within

hierarchical clustering of each cell type and representation from each patient in the individual cell clusters (Fig. S1A'-B"). Cell type annotation of Leiden clusters was based on lineage-specific markers adapted from earlier scRNA-seq studies profiling the liver^{18,24,34} (Fig. 1C,F), such as T cells (*CD3E*, *CD3D*, *IL7R*, *CD8A*, *CD8B*, *TRAC*), NK cells (*NCAM1*, *GNLY*, *NKG7*, *TRDC*, *PRF1*), myeloid cells (*CD14*, *CSF1R*, *FCGR3A*, *C1QA*, *C1QB*, *IDO1*, *CLEC10A*), B cells (*MS4A1*, *MZB1*, *CD79A*, *JCHAIN*), stellate cells (*ACTA2*, *RGS5*, *COL1A1*), endothelial cells (*PECAM1*, *RELN*, *ENG*, *FSCN1*, *CAVIN2*), and hepatocytes (*ALB*, *CYP3A4*). Importantly, we successfully captured an adequate representation of hepatocytes ($n \sim 1,850$) and neutrophils (*FCGR3B*, *CSF3R*, *S100A8*, *S100A9*) by slight modification of single-cell dissociation and sequencing methodologies. This allowed us to generate a comprehensive profile of the liver and PBMCs, and delineate changes associated with FC (Fig. 1B",D,E",G).

Initial analysis of broad cell types revealed that compared to CHB, the FC patients display a marked reduction of T cells along with a concomitant increase in NK cells and neutrophils in the intrahepatic environment (Fig. 1D). Intriguingly, we failed to observe the same trend in peripheral circulation upon analysis of PBMCs from matched patients (Fig. 1G). Notably, multiparametric flow cytometry (Fig. 1H) also confirmed the reduction in T cells and an increase in the NK/NKT population in the liver biopsies of FC patients, while the peripheral circulation failed to capture similar changes (Fig. 1I). Overall, these observations suggest that there may be specific changes in immune cell composition within the livers of FC patients that may not always be reflected accurately in PBMCs.

FC patients exhibit a marked loss of exhausted CD8 T cells and the emergence of a CD4-associated adaptive immune response

Next, we sought to determine the phenotypic changes in T and NK cell populations between FC patients and those with CHB. First, we subdivided the major T and NK clusters (identified in Fig. 1B,1B") followed by re-clustering of these cell types to reveal heterogeneity in their phenotypic states and investigated how they are altered upon FC compared to CHB. Deep phenotyping of the sub-clustered T and NK cells using cluster-specific differentially expressed genes from the scRNA-seq data (Fig. 2A,A') resulted in the identification of distinct cellular sub-types or cell states including CD4 T helper cells (*CD4*, *IL7R*, *CCR7*; Fig. S3A,B cluster 4,10), CD4 cytotoxic T lymphocytes or CD4-CTLs (*IL7R*, *KLRG1*, *PRF1*, *TNF*, *NCR3*, *GZMA*, *GZMK*; Fig. S3A,B cluster 3, 6), CD8 T effector cells (*CD8A*, *KLRG1*, *PRF1*, *KLRK1*, *IFNG*; Fig. S3A,B cluster 0), exhausted CD8 T cells (*CD8A*, *LAG3*, *FASLG*, *PDCD1*, *HAVCR2*, *TIGIT*^{high}; Fig. S3A,B cluster 5), memory-like CD8 T

cells (*CD8A*, *IL7R*, *TNF*, *IFNG*, *TNFSF10*^{high}, Fig. S3A,B cluster 11), Tregs (*FOXP3*, *IL2RA*, *CTLA4*^{high}, *BATF*^{high}, *TIGIT*, Fig. S3A,B cluster 8), liver-resident NK or LR-NK (*CXCR6*, *EOMES*, *NCAM1*^{high}, Fig. S3A cluster 1; Fig. 3A), conventional NK or cNK (*NCAM1*^{low}, *FCGR3A*, *GNLY*, *GZMB*, *PRF1*^{high}, Fig. S3A cluster 2; Fig. 3A), and NKT cells (*CD3D*, *NCAM1*^{low}, *GZMK*, *GNLY*, *PRF1*, Fig. S3A cluster 7; Fig. 3A). In particular, we noted a marked reduction in the exhausted PDCD1+ CD8 T cells and an almost complete loss of FOXP3+ Tregs in FC patients (Fig. 2A-D). The exhaustion markers such as TIGIT, LAG3 and PDCD1 are significantly reduced in FC patients (as depicted in UMAP projections in Fig. 2C, and violin plots in Fig. 2D). These changes were again mainly reflected in the liver (Fig. 2A-D), rather than in PBMCs, likely due to the lower frequency of these cells in the peripheral circulation (Fig. S4A,B"). Similarly, the decline in the frequency of FOXP3+ Tregs in FC patients compared to those with CHB was more evident in the liver (Fig. 2C). Importantly, flow cytometry analysis further corroborated these findings (Fig. 1H,I). Direct ex vivo flow cytometry analysis on global CD8 T cells in the liver also revealed a markedly lower frequency of PD1+ and TIM3+ exhausted CD8 T cells in FC patients (Fig. 2E). This was evident not only in the CD69+ tissue-resident CD8 T cells, but also in the transiting CD69- T cells. Stratifying patients with CHB based on the levels of qHBsAg showed that the reduction of exhausted CD8 T cells correlated with the reduction of qHBsAg (Fig. 2E). However, this phenomenon was not evident in the PBMC fraction (Fig. S5D; similar to what we observed in scRNA-seq data). Most notably, concomitant with the loss of exhausted CD8 T cells and Tregs, we observed a novel and distinct increase in the population of CD4 T cells that displayed markers typically associated with effector cytotoxic lymphocytes (*PRF1*, *GZMA*, *GZMK*, *TNF*, *NCR3* in Fig. 2A,A',B and Fig. 3A), hence referred to as CD4-CTLs, in patients displaying FC (Fig. 2F,F' and Fig. S3B,C). Furthermore, deep phenotyping revealed that these CD4-CTLs express markers associated with terminally differentiated, antigen-experienced CD4 T cells (*IL7R*, *KLRG1*) that display unique characteristics of inflammatory, cytotoxic effector cells including *TNF* (*TNF α*). Interestingly, they also express the *NCR3* gene resembling features of innate, NK-like cells (Fig. 2F,F' and Fig. S4D,E³⁵) suggesting a gain of innate-like function in CD4-CTLs. Notably, flow cytometry analysis also revealed increased frequency of KLRG1+ CD4 T cells both in tissue resident (CD69+) and transiting (CD69-) T cells (Fig. 2F'). Notably, a higher frequency of CD4+ KLRG1+ cells was observed in the low qHBsAg group (qHBsAg 0.05-1,000 IU/ml) compared to the high qHBsAg group (qHBsAg >10,000 IU/ml). Hence, we independently interrogated the phenotype of CD4-CTLs as a function of qHBsAg using cytometry by time-of-flight analysis on CD4 cells

the liver compartment of CHB and FC patients. (D) Percentage-based proportionality bar graph representing cell types within the liver between CHB and FC patients. (E) UMAP projection of Leiden-based clustering of ~44,396 scRNA-seq libraries generated from PBMCs of CHB and FC patients identifies 17 distinct cell states. (E') Annotation of Leiden clusters based on the top DEGs and reference-based markers identifies 8 major cell types. (E") Condition-wise annotation of scRNA-seq data from the two patient cohorts of CHB (red) and FC (blue) in PBMCs. (F) Heatmap of cell type-specific markers within PBMCs isolated from CHB and FC patients. (G) Percentage-based proportionality bar graph representing cell types in PBMCs from CHB or FC patients. (H,I) Multiparametric flow cytometry on isolated leukocytes from liver biopsies (H) and PBMCs (I) from CHB or FC patients. UMAP projection of manually gated immune populations from liver or PBMCs. Bar charts represent average relative frequency of the different immune subsets (including T cells, Tregs, and NK, NKT as well as CD56-/CD3- cells). Note: down-arrows represent a decrease whereas up-arrows depict an increase in relative proportions of individual cell types between conditions (CHB or FC). CHB, chronic hepatitis B; DC, dendritic cell; DEGs, differentially expressed genes; FC, functional cure; NK, natural killer; scRNA-seq, single-cell RNA sequencing; Tregs, regulatory T cells; UMAP, uniform manifold approximation and projection.

Single cell atlas of functionally cured CHB patients

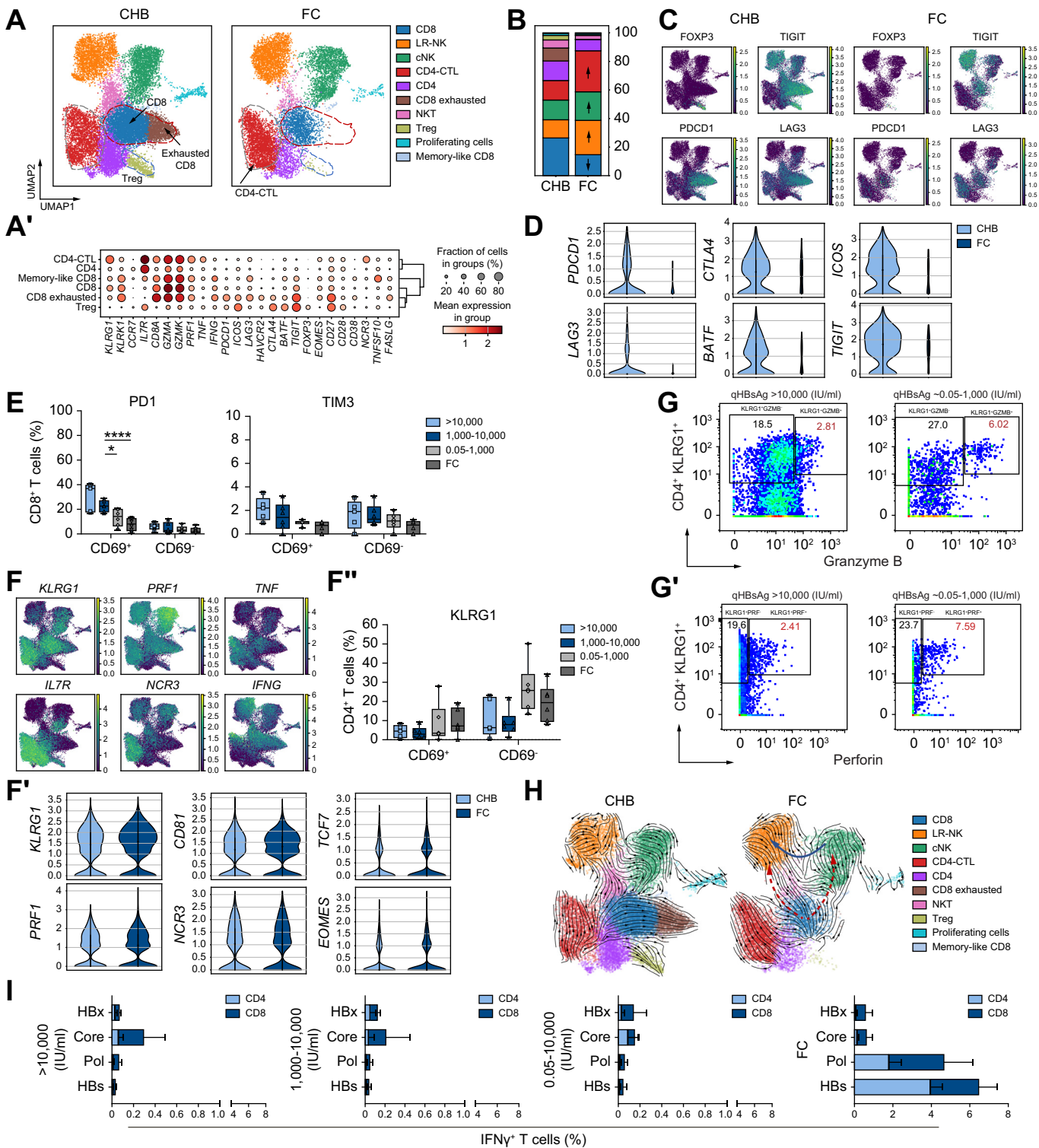


Fig. 2. Patients exhibiting FC display loss of exhaustion markers, a gain of innate and an altered adaptive immune response. (A-B) Comprehensive transcriptomic analysis of NK and T cells identified from liver tissue of CHB and FC patients. (A-A') Loss of exhausted CD8 T cells (brown cluster marked within red dashed line) and Tregs (marked by blue dashed line) in FC patients. Percentage-based proportionality bar graph summarizes the differences in composition of T-cell subsets between CHB and FC patients (B). Note: down-arrows represent a decrease whereas up-arrows depict an increase in relative proportions of individual cell types between conditions (CHB or FC). (C-D) Alterations in exhaustion markers in CHB vs. FC in the intrahepatic environment. Note the marked reduction in exhaustion markers *TIGIT*, *PDCD1*, and *LAG3* amongst the exhausted CD8 T cells and the expression of *FOXP3*+ Tregs (C). Violin plots showing expression of specific exhaustion markers *PDCD1*, *CTLA4*, *ICOS*, *LAG3*, *BATF*, and *TIGIT* between livers of CHB and FC patients (D). (E) Frequency of *PD1*+*CD8* and *CD4* T cells shown in tissue-resident (CD69+) and transiting (CD69-) populations in liver (CHB patients stratified based on qHBsAg levels). (F) Increased expression of specific effector cell markers on *CD4*-CTL clusters (*KLRG1*, *PRF1*, *TNF*, *IL7R*, *NCR3*, *IFNG*) ("red" cluster within grey dashed line in panel A) (F') Violin plots for differential expression of markers related to cytolytic function of *CD4*-CTLs (*KLRG1*, *CD81*, *TCF7*, *PRF1*, *NCR3*, and *EOMES*) between CHB and FC patients. (F'') Frequency of *KLRG1*+*CD4*+ T cells between CHB and FC patients.

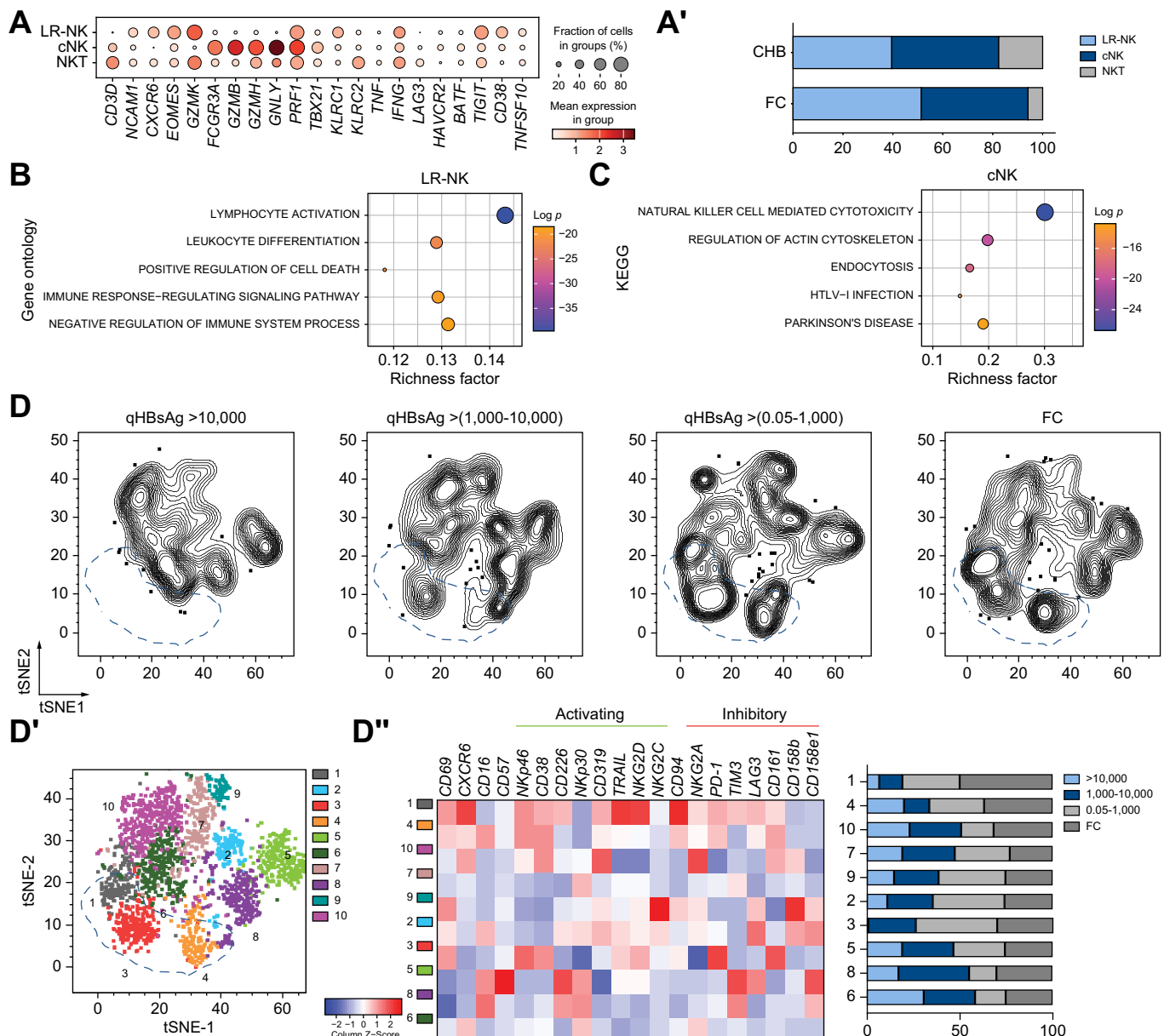


Fig. 3. FC patients display primed state for intrahepatic NK cells. (A-A') Dot plot and percentage-based proportionality chart depicting differential expression and frequencies of distinct NK cell subsets (LR-NK, cNK and NKT) within liver compartment between CHB and FC patients. (B-C) Gene ontology pathway analyses on LR-NK and cNK cells from CHB and FC patients. (D-D'') Multiparametric flow cytometry analysis on total NK cells isolated from liver. tSNE clustering (D) and PhenoGraph analysis (D') on CHB patients (stratified based on qHBsAg levels) and FC patients. Z score normalized expression of activating and inhibitory receptors in each cluster shown in heatmap (D''). Bar chart depicts frequency of each cluster in CHB patients (stratified based on qHBsAg levels) and FC patients. LR-NK, liver resident natural killer; cNK, conventional natural killer; tSNE, t-distributed stochastic neighbor embedding.

isolated from liver and matched PBMCs of two patients with CHB, exhibiting high ($>10,000$ IU/ml) vs. low (0.05-1,000 IU/ml) qHBsAg (also independently validated in two more patient samples plus healthy liver control in Fig. S5A). As shown in Fig. 2G-G', a patient with low qHBsAg displayed a ~2-3x increase in the expression of granzyme B and perforin within the

KLRG1+ CD4 population compared to the patient exhibiting high qHBsAg, further corroborating the notion that loss of qHBsAg may be associated with the emergence of CD4-CTLs. Importantly, this was observed only in the intrahepatic environment, and not in matched PBMCs (Fig. S5A), once again suggesting that changes in the intrahepatic immune

cells shown in tissue-resident (CD69+) and transiting (CD69-) populations in liver (CHB patients stratified based on qHBsAg levels). (G-G') CyTOF analysis of KLRG1+CD4+ T cells expressing granzyme (G) and perforin (G'). (H) Steady-state RNA velocity of NK and T-cell clusters in CHB and FC patients within liver compartment. Note: arrows depict the directionality of cell-state transitions. (I) Frequency of IFN γ -HBV-specific CD4 vs. HBV-specific CD8 T cells (HBs, Pol, Core and HBx). Note: qHBsAg stratification based on the following parameter: IU/ml >10,000; 1,000-10,000; and 0.05-1,000. Statistics in panel E calculated using two-way ANOVA with Tukey test, * $p \leq 0.05$, ** $p \leq 0.01$. CHB, chronic hepatitis B; FC, functional cure; LR-NK, liver-resident natural killer; cNK, conventional natural killer; T reg, regulatory T cells; CD4-CTL, CD4 cytotoxic T lymphocyte; POL, polymerase, HBs, HBsAg; HBx, HBV X.

environment may not always be adequately represented in peripheral circulation.

Trajectory analysis via RNA velocity²³ (Fig. 2H) suggested that the emergence and increase of CD4-CTLs in FC patients is most likely a result of naïve CD4 cells differentiating into CD4-CTLs, possibly under the stimulation of IL2-STAT5 signaling and IFN γ , as inferred by pathway analysis (Fig. S3D,D') and described in previous reports.³⁵ Notably, the trajectory analysis also revealed a clear demarcation between CD4-CTLs and conventional CD8 T cells even though they share common marker genes like CD8 and IL7R. Furthermore, the trajectory analysis also exposed remarkable plasticity of the CD8 T cells (Fig. 2H). We identified two populations of CD8 T cells; one that is observed predominantly in CHB (right segment of CD8 cluster), which also gives rise to the exhausted CD8 T cells, marked by the expression of *PDCD1*, *LAG3* and *TIGIT* (Fig. 2C,D). FC was marked by a striking disappearance of this exhausted CD8 T cell cluster. Intriguingly, the remaining subset of CD8 T cells revealed trajectories that suggest their transition into NKT and cNK cells. Similar observations have been made in the context of cytomegalovirus exposure where CD8 T cells were shown to gain innate-like characteristics, which was attributed to the loss of *BCL11B* expression.³⁶ Corroborating this notion, we observed a similar reduction in *BCL11B* expression in the exhausted CD8, CD8 T and memory-like CD8 T cells in the livers of FC patients (Fig. S4F). The cNK and NKT clusters in turn appear to contribute towards the LR-NK cells that are increased in FC patients, suggesting the transition from CD8 to NKT or cNK to LR-NK might promote an innate immune active state. Altogether, this data suggests the presence of an altered adaptive immune response associated with CD4-CTLs expressing effector proteins (*PRF1*, *GZMA*, *IFNG*, *TNF*) and pathways such as IL2, STAT5; and also highlights the plasticity of T cells to acquire innate-like features and likely, function.^{37–40} mIF staining with a panel of antibodies against activated T cells (CD3, GZMB and Ki67; T-act panel from Ultivue) on FFPE sections cut from biopsies of the same patients further validated the decline in T cells, increase in proliferating cytotoxic T cells and an increase in GZMB+ cells associated with FC (Figs S3E,E' and S12). Altogether, these observations suggest that the emergence of CD4-CTLs coupled with gain of NK-like innate immune characteristics in both CD4-CTLs and CD8 T cells, may drive a shift in the intra-hepatic environment from an immune-suppressed to an immune-active state in FC patients.

Emergence of antigen-specific CD4 T cells with robust effector function as key regulators of viral clearance in patients exhibiting FC

Next, we utilized flow cytometry to comprehensively characterize the phenotype of global CD8 and CD4 T-cell populations found within the liver and PBMCs of patients with CHB (n = 17) vs. those exhibiting FC (n = 6) (profiled at the same time as scRNA-seq samples) (Fig. S5B-E). Specifically, we explored whether the phenotypic changes in CD4 or CD8 T-cell populations correlated with qHBsAg levels since we observed a strong positive correlation between HBV DNA levels and qHBsAg levels (Fig. S2A). As depicted in Fig. S5B,D, tissue-resident (CD69+) CD4 and CD8 T cells showed an increased frequency of markers of memory-like T cells (CD127+), loss of senescence (CD57+) and terminal differentiation (HLA-DR+).

Surprisingly, unlike peripheral CD4 T cells which showed somewhat similar phenotypic changes to those found in the liver compartment, no loss of senescence in CD8 T cells was observed (Fig. S5C,E). Once again, these observations revealed distinct differences not only in the robustness of the immuno-phenotypic changes, but also in the patterns observed between the two tissue types (liver vs. PBMCs). Loss of exhaustion and senescence combined with an increase in memory-like T cells suggests a gain in effector phenotypes and proliferative capacity in CD4 and CD8 T cells in the absence of viral antigens in FC patients.^{41,42}

During the natural history of HBV infection, HBV-specific T cells, specifically CD8 T cells, are associated with viral control. Given the observed altered adaptive immune response in the liver based on scRNA-seq, we asked whether HBV-specific T-cell responses differ between CHB and FC patients. Due to limitations in acquiring intrahepatic samples, HBV-specific T cells were analyzed in PBMCs (CHB n = 12, FC n = 5) at the time of biopsy as shown in previously published studies.^{19,43} Deconvolution of the HBV-specific T-cell repertoire, using ELISpot, demonstrated that the HBV-specific responses are peptide-specific in both CHB and patients achieving FC. Interestingly, while patients with CHB displayed HBV core and HBx-specific T cells, there was a distinct increase in the HBsAg (HBs)- and HBV polymerase (Pol)-specific T cells in FC patients (Fig. S6A). Remarkably, further analysis by intracellular cytokine staining demonstrated that in patients exhibiting FC, the HBV-specific T cells are largely contained within the CD4 T-cell population, with HBs-specific CD4 T cells being present at a higher frequency than the corresponding CD8 T cells (Fig. 2I). Notably, a recent study identified higher frequencies of HBV-specific CD4 T cells in acute resolved and FC patients compared to patients with CHB, corroborating our observation of a dominant HBV-specific CD4 response.⁴³ Furthermore, HBs-specific CD4 T cells showed a higher degree of multi-functionality, as measured by IFN γ /TNF α secretion in FC patients (Fig. S6B). Notably, core- and HBx-specific CD8 T cells were identified among all patients with CHB, albeit at low frequencies, regardless of qHBsAg levels (Fig. 2I). However, FC patients displayed an increase in pol- and HBs-specific CD8 T cells. More importantly, HBV-specific CD4 T cells (mainly pol and HBs-specific) were observed exclusively in patients exhibiting FC (Fig. 2I), suggesting the importance of a robust effector function in certain peptide-specific T cells in the long-term maintenance of FC.

Intrahepatic NK cells display a primed state in FC patients

In addition to the increase in CD4-CTLs, FC patients also displayed an increase in the classical innate immune response. Analysis of liver scRNA-seq data showed a distinct increase in the LR-NK cells (*CXCR6*, *EOMES*) (Fig. 3A,A'), which have been suggested to perform a more immune regulatory role by secreting cytokines and engaging with signaling interactions with various cell types, such as recruiting DCs to the site of inflammation and promoting cross presentation of antigens to remodel the liver environment.^{44–47} FCGR3A+ cNK cells, which are directly involved in antibody-dependent cellular cytotoxicity⁴⁸ and known to promote anti-viral T-cell responses,⁴⁷ also show a mild increase in FC patients (Fig. 3A,A'). As shown in Fig. 3B,C, pathway analysis on gene expression signatures

strongly suggested an increase in immune effector function in both cell types with specificity towards cytokine-chemokine secretion in LR-NK and antibody-dependent cellular cytotoxicity in cNK cells. Furthermore, direct *ex vivo* flow cytometry analysis in the liver revealed a gradual enrichment of CXCR6+ CD69+ NK clusters with declining levels of qHBsAg (Fig. 3D). These cells displayed elevated expression of activating receptors (NKP46, CD38, NKG2D and TRAIL) (Fig. 3D',D'', and Fig. S6E) and lower expression of inhibitory receptors, such as PD1 and TIM3 in FC patients (Fig. 3D',D'', and Fig. S6F). We suggest that the CXCR6+ CD69+ NK cells are representative of the LR-NK cells identified in the scRNA-seq analysis and have been described in earlier studies.^{44,45} That said, some of the LR-NK cells in FC patients also displayed moderate-to-high expression of other inhibitory receptors, such as PD1 and LAG3 (Figs 3D' and S6E,F). Based on these markers we identified CD69+ CXCR6^{high} CD16- (Fig. 3D', cluster 1) and CD69+ CXCR6^{low} CD16+ (Fig. 3D', cluster 4) populations that emerged with declining HBsAg levels and were enriched in FC. These populations are characteristic of the LR-NK and cNK respectively, as identified in scRNA-seq data (Fig. 3D). Interestingly we also identified another population marked by CD69+ CXCR6- CD16- that was enriched with low qHBsAg levels (Fig. 3D',3D'', cluster 3). Altogether, multiparametric flow cytometry data suggests that the effector cytotoxic function of tissue-resident NK cells must be carefully moderated by the balanced expression of activation and inhibitory receptors. Similar analysis on PBMCs (Fig. S7A-D) revealed enrichment of CD56^{dim} clusters consisting of mature NKs (CD16^{high}, CD57^{high}) or with high expression of activating receptors (NKP30, TRAIL, and CD38) and lower inhibitory receptors (PD1, TIM3) in FC patients (Figs S7B-D). We assessed whether the liver immune environment in FC patients reverts to healthy liver conditions by mining previously published scRNA-seq data of healthy liver²⁴ and Harmony-based integration of healthy liver data with our scRNA-seq data from CHB and FC patients. We observed that the LR-NK and cNK cells from FC patients display features of low-grade immune-active states that are distinct from the transcriptomic states found in healthy livers (Fig. S13A,A') despite similarities observed in frequencies of cNK/LR-NK cells between FC and healthy livers (Fig. S13A''). These observations suggest a gradual but inverse trend of increased activated NK cell function with decreasing qHBsAg levels, which highlights a biological gradient of enhanced innate immune function associated with FC.⁴⁸

Remodeling of intrahepatic myeloid environment into an immune-active state in FC patients

Thus far, our data suggest a gradual shift towards an immune-active state within the liver of FC patients. To understand the systemic immune response in patients, we analyzed plasma cytokines, chemokines, and soluble receptors by Luminex. Plasma analysis showed that there is a gradual yet mild increase in pro-inflammatory cytokines and chemokines like IL-1 β , ENA-78 (CXCL5), BAFF and MCP-1 (CCL2) with decreases in qHBsAg levels (Fig. S2B). Amongst these, ENA-78, an epithelial neutrophil attractant protein is known to be produced by endothelial cells to recruit neutrophils, T and B cells and eosinophils to the liver compartment,⁴⁹⁻⁵¹ indicating low-grade inflammation in FC patients. Indeed, neutrophils represent a crucial component of the intrahepatic myeloid cell population

that constitute the first line of defense against pathogens. There is increasing evidence for neutrophils serving as long-term modulators of innate immunity and their role in altering the immune environment during viral infection and resolution.⁵²⁻⁵⁴ Therefore, we explored alterations in the nature and composition of neutrophils, both in whole blood and liver compartments of CHB vs. FC patients. As shown in Fig. 4A,A' and Fig. S9A-A'', the whole blood compartment had lower overall neutrophil frequencies in FC patients. However, a mature sub-population, highlighted by cluster 4 (Fig. 4A-A''), appeared to increase in frequency in FC patients. Across the different whole blood neutrophil subsets (Fig. S9B), there was a general decline in neutrophil recruitment markers in FC patients (Fig. S9C). Nonetheless, the whole blood cluster 4 neutrophils exhibited high levels of DUSP1, PTGS2, CEBPB, ISG15, IFIT3, IFITM1, and IFITM3 in FC patients (Fig. 4B and Fig. S9D,E). Upregulated pathways showed TNF α signaling via NF- κ B, interferon (IFN) response, regulation of cytokine production, increased response to virus and pattern recognition receptor pathways in FC (Fig. 4B',B'' and Fig. S9F). In contrast to what we observed in whole blood, the liver compartments of FC patients showed higher numbers of neutrophils compared to CHB (Fig. 4C,C'', Fig. S10A-A' and B). The enrichment in neutrophils could be attributed to the phenomenon of neutrophil infiltration and margination observed frequently in the context of lung disease and in other tissues.^{52,55,56} Pathway analysis showed that neutrophils within the liver from FC patients may play a role in leukocyte differentiation and TNF α signaling via NF- κ B (Fig. S10C). These marginated neutrophils exhibited higher levels of CXCR2, CXCL8, LYZ, NCF1, NAMPT in FC patients (Fig. S10D). Additionally, we identified increased CXCR4-CXCL12 interactions and decreased CXCR1/2-CXCL2 interactions (inferred cell-cell interactions; Fig. 4D and Fig. S10F,G) between neutrophils and endothelial cells (sub-clustering of endothelial cells; Fig. S10E), implying increased neutrophil trafficking and their long-term residence within the liver compartment in FC patients. The decline in IFN-stimulated genes in FC neutrophils (Fig. 4E) suggests that they may no longer be actively engaged in eliciting an innate response. However, it is tempting to speculate that these populations may retain their capacity to secrete key cytokines to signal effector cells (CD4/CD8 T cells, NK cells) to clear the virus in case of repeated exposure during reactivation.

Furthermore, we analyzed the expression of inflammatory genes in myeloid populations in Harmony-integrated healthy liver from MacParland et al.²⁴ and compared it with our scRNA-seq data from CHB and FC patient livers (Figs. S13B-B'' and S8A-C, respectively). We observed that the myeloid populations of FC patients display distinct levels of pro-inflammatory and immune-active genes (*IL1B*, *TNF*, *IFNG*, *TGFB1*, *NFKB1*, *IL6* and *CD80*), whereas the expression of anti-inflammatory genes, such as *IL10* appears to be much lower in FC patients compared to CHB and healthy livers. Additionally, single-cell profiling of myeloid cells also suggested a distinct remodeling of the liver environment of FC patients into an immune-active state as evidenced by an increase in CD14+ classical monocytes, and a decrease in CD16+MARCO+ non-classical monocytes (Fig. S14A,B). Direct *ex vivo* flow cytometry analyses confirmed the increase in CD14+ pro-inflammatory monocytes in the liver of FC patients (Fig. S14C), indicating an ecosystem of low-grade immune activity. We also observed a distinct enrichment of

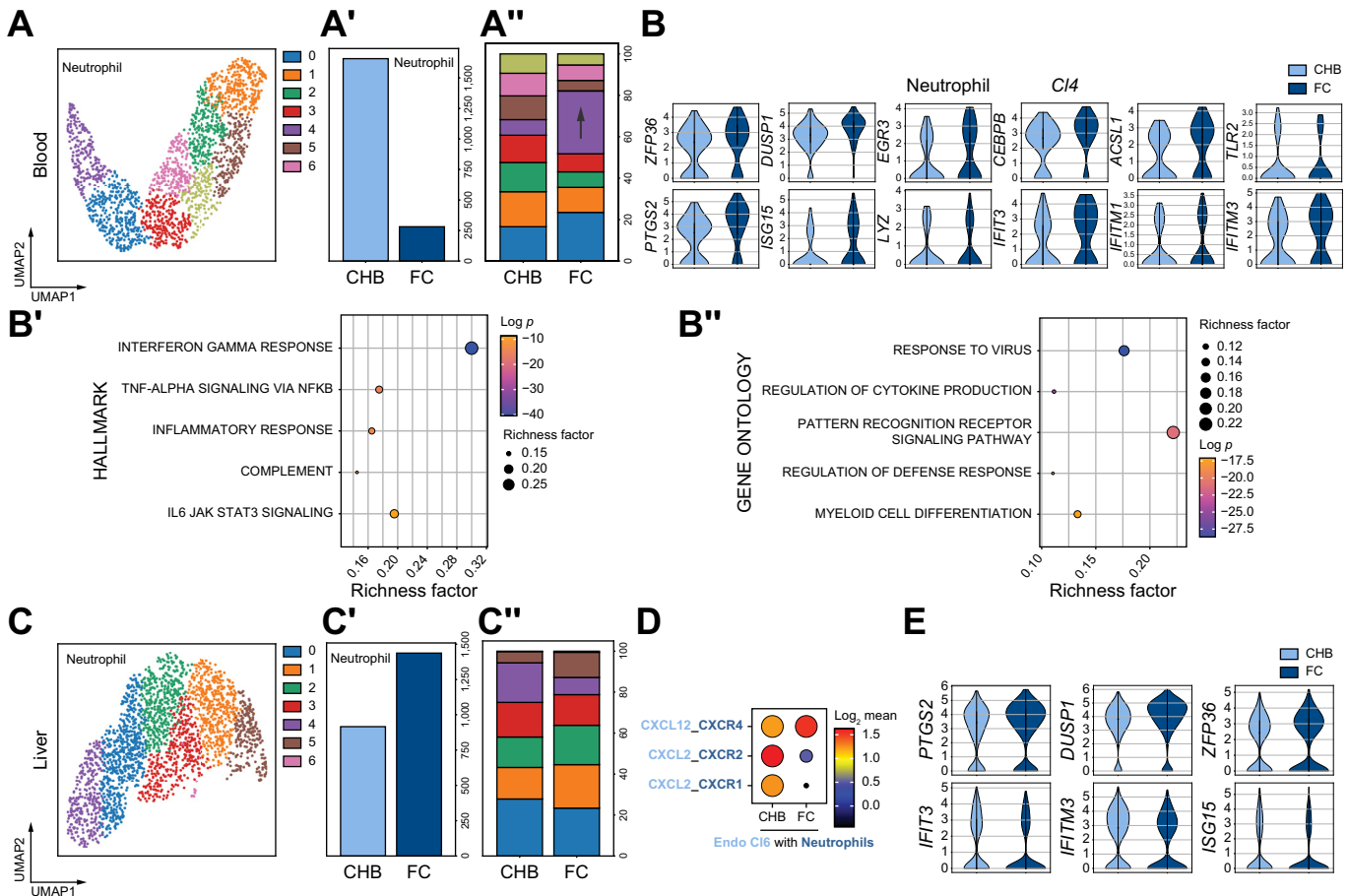


Fig. 4. Presence of margined neutrophils within the liver of FC patients. In-depth characterisation of the transcriptomic profile of sub-clustered neutrophils isolated from whole blood (A-B'') and intrahepatic environment (C-E), between CHB and FC patients. (A) Clustering of neutrophils in whole blood indicates 8 different cell states. (A') Frequency of neutrophils in CHB vs. FC patients. (A'') Percentage-based proportionality bar plot showing increased frequency of neutrophil c14 (purple) in FC patients. (B) Violin plots highlighting differential expression of neutrophil c14-associated markers (*ZFP36*, *DUSP1*, *EGR3*, *CEPB*, *ACSL1*) including pro-inflammatory markers (*TLR2*, *PTGS2*, *ISG15*, *LYZ*, *IFIT3*, *IFITM1*, and *IFITM3*), between CHB and FC patients. (B'-B'') Hallmark (B) and gene ontology (B'') annotation-based identification of pathways upregulated in FC patients that are specifically associated with cluster 4 neutrophils from whole blood. (C) Clustering of neutrophils in liver shows 7 distinct cell states. (C') Bar chart depicts increased frequency of neutrophils in liver from FC compared to CHB. (C'') Percentage-based proportionality bar plot showing differential frequency of specific neutrophil populations in FC patients. (D) CellPhoneDB-based inference of altered cell-cell interactions between neutrophils and endothelial cell cluster 6, such as CXCL12-CXCR4; CXCL2-CXCR1; and CXCL2-CXCR1, between CHB and FC patients. (E) Violin plots quantifying differential expression of neutrophil markers (*DUSP1*, *PTGS2*, *ISG15*, *IFIT3*, *IFITM1*, *IFITM3*, and *ZFP36*) between CHB and FC patients. Statistical analysis utilized two-way ANOVA with Tukey test. * $p \leq 0.05$. CHB, chronic hepatitis B; FC, functional cure; C14, cluster 4.

DC2 (Fig. S14B, supported by flow validation in Fig. S14C,C') and *FOLR2/VSIG4* KC populations in FC patient liver Fig. S14B. CellPhoneDB analysis revealed that both DC2 and *FOLR2/VSIG4* KC populations display robust inferred interactions with CD4-CTLs and memory-like CD8 cells (Fig. S8E-E'), thereby suggesting their putative function in eliciting an active immune response. Interestingly, the *FOLR2/VSIG4* KC subtype was found to express *TIMD4*, *ADGRE* (F4/80), *MRC1* and *CD36* (Fig. S14D,E), reminiscent of the IL2-dependent "KC2" subtype reported by De Simone et al.,¹³ where the KC2 subtype was shown to have the ability to cross-present antigens to reinvigorate a defective effector response in mouse models of HBV infection.¹³ Taken together, our data underscores an important function of myeloid cells in modulating a shift from an anti-inflammatory to an immune-active environment, perhaps by regulating increased viral antigen presentation and re-education of effector cells through the *FOLR2/VSIG4* KCs. Importantly, our data highlights a previously unappreciated role for neutrophils as important mediators of sustained viral clearance in FC patients,

and further supports the hypothesis that enhanced innate immune responses may play an important function in achieving FC.

Identification of MHC class II-expressing hepatocytes in patients displaying FC

Profiling of the immune cells in the livers of FC patients revealed a pro-inflammatory switch in the liver environment with increased innate immune response via LR-NK, cNK, and neutrophils; increased antigen presentation via specific KCs that could educate CD4 and CD8 T cells; and the emergence of CD4-CTLs that could be activated by pro-inflammatory stimuli (IL2, TNF, IFNG) and educated by KCs. The key question that remained was how the CD4-CTLs or HBV-specific T cells effectively target the hepatocytes presenting viral antigens in FC patients. In order to gain further insights, we decided to probe deeper into hepatocytes, which have generally eluded most single-cell approaches on the liver environment. In this study, we successfully profiled an adequate number of hepatocytes (n

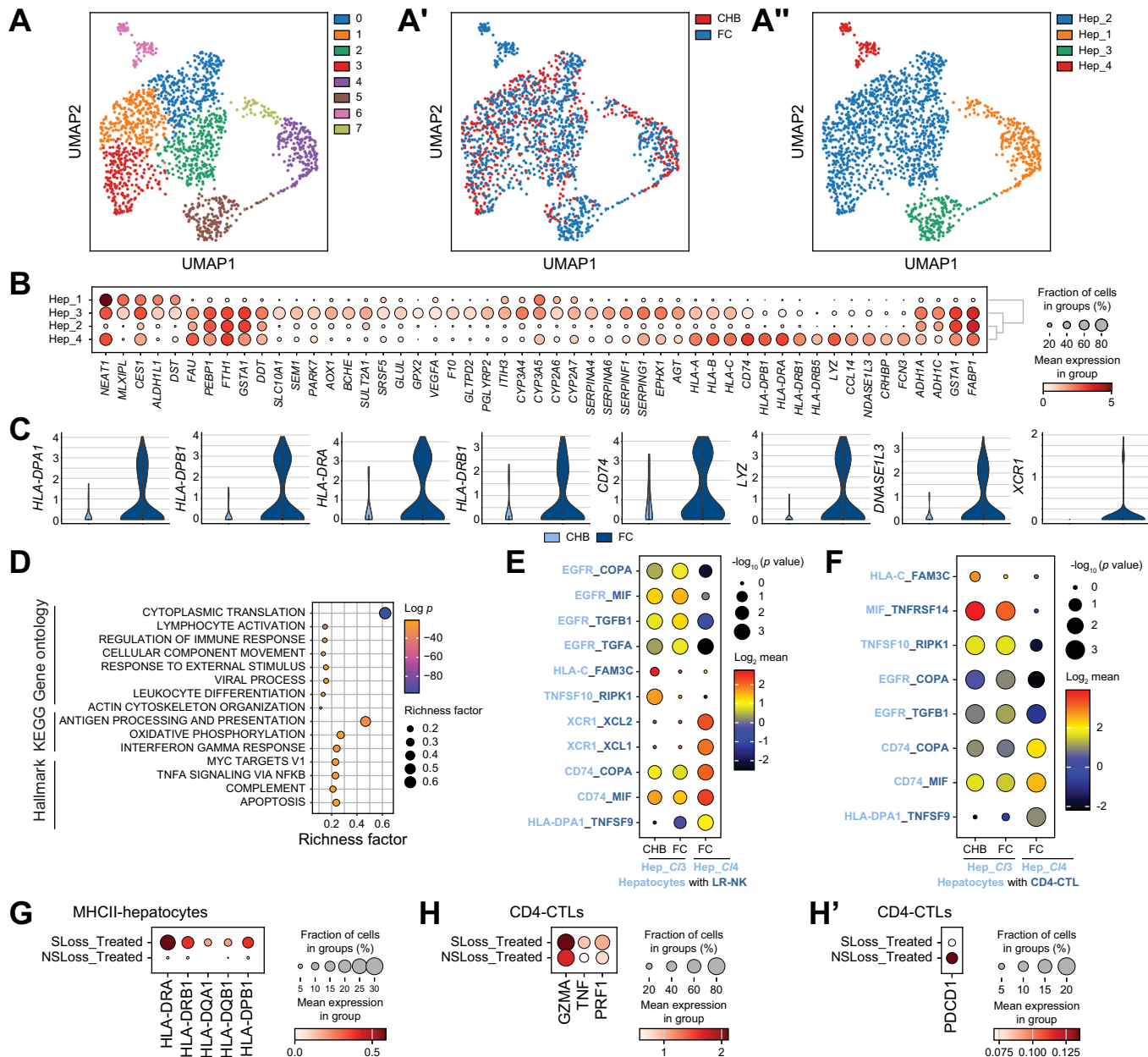


Fig. 5. Increased MHC class II expression in hepatocytes in patients exhibiting functional cure. (A-A') Transcriptomic analysis and sub-clustering of hepatocytes based on scRNA-seq data from liver of CHB and FC patients. Leiden clusters identify 8 distinct sub-clusters, cell states within hepatocytes (A); condition-wise (CHB vs. FC) labelling of Leiden clusters (A'); identification of 4 major cell states based on top DEGs (A'). (B) Dot plot of DEGs amongst the 4 major hepatocyte cell states/clusters identified in A'. Note higher expression of MHC class II-related genes in Hepatocyte clusters Hep_3 and Hep_4 including CD74, HLA-DPB1, HLA-DRA, HLA-DRB1 and HLA-DRB5. (C) Violin plots highlighting differential expression of MHC class II-related genes (HLA-DPA1, HLA-DPB1, HLA-DRA, HLA-DRB5, CD74) in hepatocytes between CHB vs. FC patients. (D) Pathway analysis based on gene ontology, KEGG and Hallmark-based annotation of genes upregulated in hepatocytes isolated from FC patients. (E) CellPhoneDB-based inferred cell-cell interaction analysis between Hep-3 and Hep-4 clusters and LR-NK populations in CHB vs. FC patients. (F) Cell-cell interaction analysis between Hep-3 and Hep-4 clusters and the CD4-CTLs isolated from the liver compartment of CHB or FC patients. Ligand-receptor genes derived from hepatocytes are labelled in Red, genes derived from either LR-NK cells (E) or CD4-CTLs (F) are labelled in Blue. Dot sizes correlate with increased significance of predicted interactions. Dot colors indicate Log base 2 of mean expression of ligand-receptor pairs of genes. (G) Dot plots of MHC class II genes expressed in hepatocytes from treated FC (SLoss) vs. treated CHB (non-SLoss or NSLoss) patients. (H-H') Dot plots of effector-activation marker genes (H) or exhaustion markers (H') in CD4-CTLs from treated SLoss vs. NSLoss patients. CHB, chronic hepatitis B; FC, functional cure; Hep, hepatocyte; CD4-CTL, CD4 cytotoxic T lymphocytes; UMAP, uniform manifold approximation and projection.

~1,850) from 15 CHB and 8 FC patients. One of the striking observations upon Leiden clustering of hepatocytes was a subset of hepatocytes (hepatocyte cluster 4 in Fig. 5A-A'') that appeared to be specifically associated with FC patients. Surprisingly, characteristic profiling of cluster 4 indicated high expression of MHC class II (MHC II) molecules in addition to

HLA-A, HLA-B and HLA-C expression (Fig. 5B,C). MHC II-high hepatocytes were also found across cluster 3 and 2 but they were predominantly associated with FC patients (Figs S11A-D and S12). Overall, a larger number of hepatocytes had a lower MHC I/II ratio in FC patients (Fig. S11D). Incidentally, IFN treatment has been reported to induce MHC II expression

in vitro and in mouse models.^{57–59} A switch in the MHC I/II ratio has also been observed in other viral-associated diseases such as Epstein-Barr virus-associated nasopharyngeal and gastric cancers.^{60,61} While upregulation of MHC II has previously been reported in human hepatocytes,⁵⁷ this is the first example of this phenomenon in the context of FC of CHB. Pathway analysis showed increased cytoplasmic translation, antigen presentation and processing, apoptosis, signals for leukocyte differentiation and lymphocyte activation among others in the MHC II-high hepatocytes (Fig. 5D and Fig. S11E,F). CellPhoneDB analysis inferred decreased interactions of HLA-C-FAM3C, EGFR-MIF, EGFR-COPA, and increased interactions of XCR1-XCL1/2, HLA-DPA1-TNFSF9, CD74-COPA, CD74-MIF between the hepatocytes and LR-NK cells or CD4-CTLs in FC patients (Fig. 5E,F). Importantly, patients who remained HBsAg positive even after treatment with NUC± IFNa (Table 1), displayed markedly reduced expression of MHC II genes compared to FC patients (Fig. 5G). Concomitantly, patients who remained HBsAg positive after treatment also displayed dysfunctional, exhausted CD4-CTLs with lower expression of effector proteins, such as GZMA, PRF1 and TNF (Fig. 5H), and significantly higher expression of checkpoint genes compared to FC patients (Fig. 5H'). Altogether, the data suggests that MHC II-high hepatocytes with enhanced cell-cell interactions with LR-NKs and activated CD4-CTLs may trigger a targeted immune response to sustain long-term control of CHB.

The notion of MHC II-mediated antigen presentation by the hepatocytes is intriguing, especially in the context of FC patients. We wondered whether there is low level of residual HBsAg being synthesized from integrated DNA or very low residual active cccDNA that may be masked by anti-HBs antibodies, and hence not easily detected by qHBsAg assays. Remarkably, virological investigation by ddPCR in the FC patients revealed a 50-fold lower but persistent level of cccDNA in their liver biopsies, compared to CHB (Fig. 6A). Additionally, despite the low levels of cccDNA, HBV DNA (Fig. 6B), and 3.5 kb HBV RNA (Fig. 6C) in FC patients, the ratio of the 3.5 kb HBV RNA to cccDNA in FC patients was found to be similar to that observed in CHB (Fig. 6D). Moreover, single-cell cDNA amplification of viral sequences enriched using HBV bait capture (see methods for detail) corroborated the results from ddPCR (Fig. 6E-H and Fig. S15). Specifically, upon mapping to the patient-matched viral genotypes (Fig. 6E-H, and Fig. S15), we found viral transcripts to be expressed both in CHB (representative examples in Fig. 6E,F) as well as FC (Fig. 6G,H) hepatocytes. As expected, the level of viral transcripts expressed in hepatocytes isolated from FC samples was ~100-1,000x lower than in CHB. Overall, these data indicate that residual cccDNA in FC patients can be actively transcribed to support low-level persistent viral replication in a few hepatocytes.

Discussion

There remains a significant knowledge gap in our understanding of the underlying immune-pathological events, especially within the intrahepatic tissue, occurring in patients who achieve FC. This can be largely attributed to the relatively low percentage of FC patients (whether treatment-naïve or under lifelong antiviral therapy), as well as limited access to their liver tissue. Moreover, the distinctive features of the liver

cannot be completely captured by profiling the readily accessible PBMC samples, which further widens this knowledge gap.^{3,17,62} A systematic investigation is therefore warranted to identify not only distinct immune-pathological cell states that are relevant to the disease, but also potential signatures that correlate with disease resolution, and eventually FC. In this study, through a comprehensive single-cell profiling of both liver and matched PBMCs isolated from CHB vs. FC patients, we identified both convergent and divergent gene expression-based DACS that may be reflective of mechanisms and biomarkers of FC.

Even though our dataset has been generated from a spectrum of patient samples from different phases of CHB and from FC (Table 1), we identified two common and important denominators. First, there are profound differences in the DACS and molecular signatures identified between the liver and peripheral circulation. While there is convergence in the global T and NK cell response (Fig. 1-3 and Fig. S3-S7), emergence of pro-inflammatory innate immune response (neutrophils and LR-NK cells) (Figs. 2-4), and increased frequencies of specific FOLR2/VSIG4 KC and DC2 subtypes (Figs. S8 and S14) were only detectable in the liver, thereby making intra-hepatic studies indispensable for the accurate identification of DACS associated with FC. Recent studies also underscore the importance of interrogating the liver environment to identify distinct DACS specific to the liver environment that may otherwise be missed by exclusively analyzing PBMCs.^{16,62–65} Second, we identified a shift in the immunological profile of the liver from an immune-suppressed environment found in patients with CHB to an immune-active environment in FC patients. Such immune remodeling could occur due to increased neutrophil infiltration and margination within the liver (Fig. 4C,C'). Additionally, an increased frequency of LR-NK cells with high expression of activation receptors (CD38, TRAIL, NKp46, NKG2D) and moderate levels of inhibitory receptors (PD1, TIM3) (Fig. 2B, and LR-NK cluster in Fig. 3A) was observed long after the loss of HBsAg. We speculate that these primed NK cells with memory-like features^{66–69} might retain their capacity to elicit a coherent immune response when re-exposed to the virus, or during long-term viral suppression.^{40,67,70–72} These immune-active states in FC patients may provide a surveillance mechanism to support the maintenance of the “functionally cured” state.

One of the most important findings was the emergence of a novel atypical adaptive immune landscape in FC patients as defined by CD4-CTLs (GZMA, PRF1) (Fig. 2 and Fig. S3). Importantly, HBV-specific T-cell analysis revealed HBs-specific CD4 T cells are in greater abundance (Fig. 2I) and elicit a stronger antiviral response (TNF α and IFN γ secretion; Fig. S6B), than the respective CD8 T cells, suggesting a role for effector CD4 T cells in FC as seen in a recent study by Hoogeveen *et al.*⁴³ Innate immune cells (including monocytes, tissue-resident macrophages like KCs, and DCs) are known to regulate adaptive immune responses in the control of CHB. Recently De Simone *et al.*¹³ showed that a “KC2” cluster, similar to the FOLR2/VSIG4 KCs identified in our study, acts in response to IL2 stimulation to reinvigorate adaptive immune subsets, especially dysfunctional CD8 T cells to resolve CHB infection in animal models.^{13,53,54,73} It is enticing to suggest that the altered pro-inflammatory myeloid signature together with increased frequencies of FOLR2/VSIG4 KC, TREM2 KC, and DC2 clusters

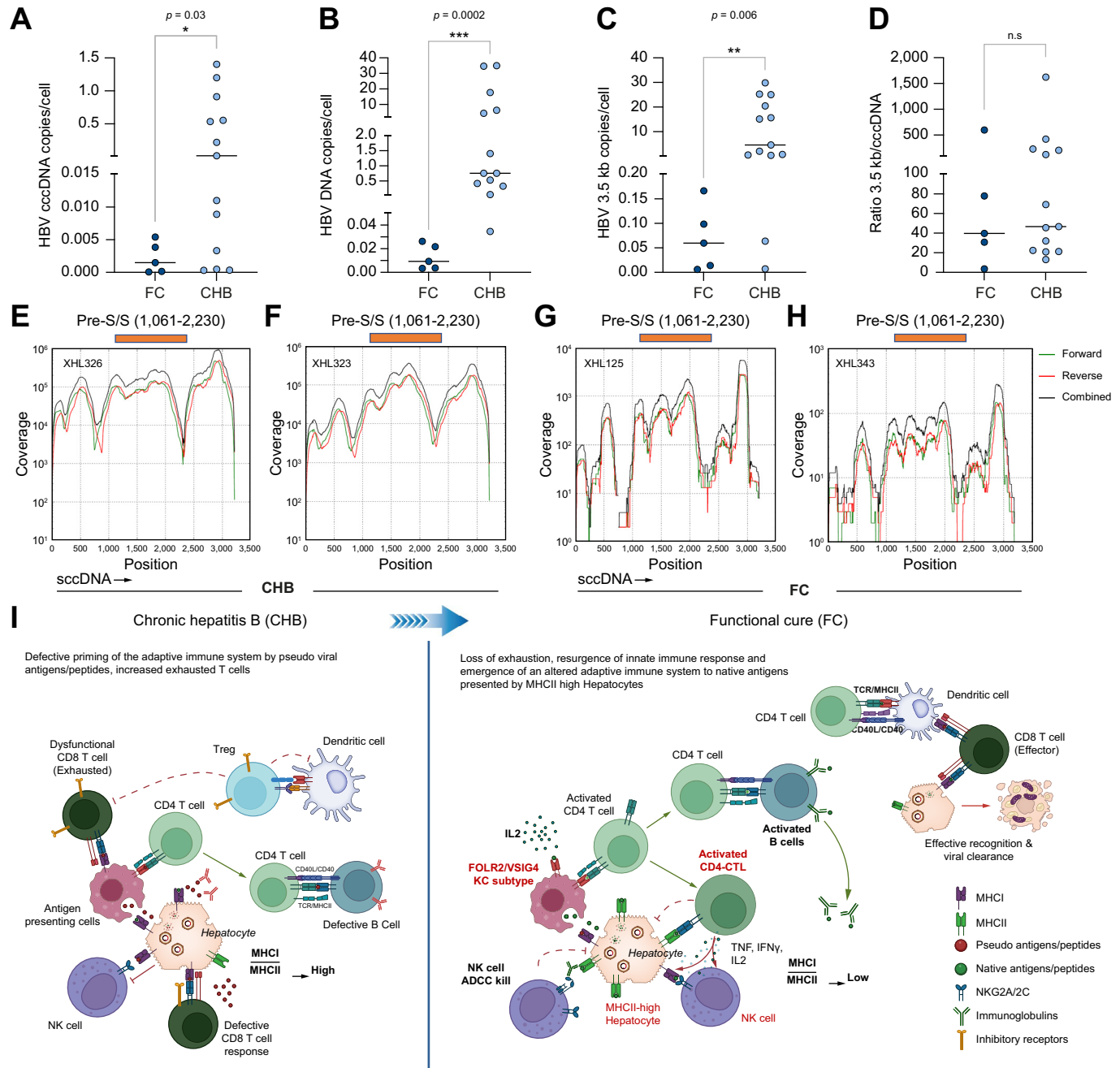


Fig. 6. Presence of low levels of cccDNA and viral transcripts within hepatocytes of FC patients. (A-D) Plots indicate HBV cccDNA copies/cell (A), HBV DNA copies/cell (B), HBV 3.5 kB RNA copies/cell (C) and ratio of HBV 3.5 kB RNA to HBV cccDNA per cell (D) as measured by ddPCR. Statistical significance was assessed by the two-tailed Mann-Whitney U test. * $p < 0.05$, ** $p < 0.01$, *** $p < 0.005$. (E-H) Viral mapping using ViPR pipeline demonstrates presence of viral transcripts in FC patients XHL125 (G) and XHL343 (H) similar to CHB patients XHL326 (E) and XHL343 (F) albeit at a lower magnitude. (I) Proposed working model illustrating the differential immune response in CHB vs. FC patients and putative mechanisms that may drive resolution of CHB and long-term maintenance of FC. CHB, chronic hepatitis B; FC, functional cure; cccDNA, covalently closed circular DNA; CD4-CTL, CD4 Cytotoxic T lymphocytes; Treg, regulatory T cell; NK, natural killer.

in FC patients, may also promote their engagement with the CD4-CTLs (Figs. S8E-F and S14) to reinvigorate an altered immune response.

In the context of a reformed immune response in FC patients, it is interesting to note that the loss of viral antigens correlated both with the emergence of CD4-CTLs and memory-like NK cells. Incidentally, plasma cytokine analysis revealed a very modest but increasing trend in IL2 expression in patients with lower HBsAg and FC (Fig. S2B). Additionally,

single-cell analysis identified CD4 T and NKT cells as potential sources for IL2 expression, which also appeared to show a mild but consistent increase upon HBsAg loss (Fig. S3A'). In the light of these results, we hypothesize that IL2 produced by a small number of T cells may be involved in priming NK cells. Previous studies have demonstrated that CD4 T cell-derived IL2 is a potent adjuvant of NK cell priming⁷⁴⁻⁷⁶ and is important for efficient IFN γ production by NK cells.⁷⁷⁻⁷⁹ Based on these findings, we speculate

that CD4 T cells may promote priming and proliferation of NK cells in the liver of FC patients to enhance innate immune activation.

Recent studies suggest CD4 T cells, apart from their helper T-cell function, can perform a supplementary role as effector T cells^{35,62,80,81} especially in situations where the underlying disease condition presents itself with a lower MHC I/II ratio driving towards MHC II-dependent antigen presentation and processing.^{82,83} The striking HBV-specific CD4 increase in resolved CHB may compensate for the inadequate immune response arising from dysfunctional HBV-specific CD8 T cells, most of which are likely exhausted by chronic exposure to pseudo-antigens produced by the virus (HBeAg and different splice isoforms of HBsAg).^{84–86} This could be explained by the chronically exhausted molecular signature within HBV-specific CD8 T cells that remain as a ‘molecular scar’, as also observed in HCV-specific terminally exhausted CD8 T cells.^{87–90} However, in certain contexts, the effector function of CD8 T cells can be restored as shown in earlier studies^{87–89} and such a restoration of effector function was observed with respect to peptide-specific CD8 and CD4 T cells in our study (Fig. 2I). In line with our observations of increased effector CD4-CTL characteristics in FC patients and given their documented association with lower MHC I/II ratios,^{58,59,82} we were intrigued by the identification of hepatocytes specifically in FC patients that displayed markedly upregulated MHC II genes (Fig. 5 and Fig. S11). This could be a function of IFN α therapy as previous studies on hepatoma cell lines, infected primary human hepatocytes, and in animal models have demonstrated upregulation of MHC II genes upon IFN α treatment.^{57,59,91,92} Similar to what was shown by Koch and Leffert⁹³ in IFN-treated animals, we observed an upregulation of the invariant chain CD74, a critical molecule in MHC II antigen presentation and processing,^{93,94} specifically in hepatocytes isolated from FC patients. It is also important to note that a majority of our FC patient cohort ($n = 7$) received a combination of NUC therapy and IFN α . This is in agreement with and could provide insights into potential mechanisms that could explain previous observations from clinical trials that demonstrated that Peg-IFN α -induced innate immune activation directly benefited from NUC therapy-driven suppression of viral replication.⁹⁵ Notably, patients who remained resistant to NUC±IFN α treatment did not present any of the immunopathological cell states associated with FC/HBsAg loss, including activated CD4-CTLs and MHC II-expressing hepatocytes (Fig. 5G–H'). Taken together, our data suggests that reduction in viral load upon NUC therapy combined with the activation of MHC II genes (in hepatocytes) by IFN α , and the emergence of CD4-CTLs may improve therapeutic outcomes in patients with CHB.

Finally, the role of MHC II-expressing hepatocytes as an accessory APC and its inferred interactions with LR-NK cells and CD4-CTLs is both novel and intriguing. There is indeed a growing body of evidence for epithelial cells expressing

increased levels of MHC II genes in multiple tissues, such as intestinal cells,^{96,97} alveolar epithelial cells,⁹⁸ and even hepatocytes,⁵⁸ that enhance presentation of antigens especially under virus-driven chronic disease states.⁹⁹ Corroborating this notion, ddPCR as well as single-cell cDNA amplification of RNAs isolated from hepatocytes revealed that FC patients (displaying HBsAg loss) continue to express viral transcripts, albeit at very low levels compared to patients with CHB (Fig. 6A–H). Notably, not only do these results provide the first direct evidence for the presence of transcriptionally active cccDNA in FC patients, but also suggest that loss of S-antigen detection in the serum may not equate to loss of S-transcript production in hepatocytes. Taken together, mechanistically, we are tempted to speculate that the balance of MHC I/II ratio could dictate the nature of immune responses observed in patients with CHB vs. those with FC (working model shown in Fig. 6I). Earlier studies suggested heterogeneity in antigen presentation by HBV-infected hepatocytes could trigger differential effector responses in epitope-specific CD8 T cells^{100–102} and in the regulation of CD4 T-cell responses.¹⁰³ We hypothesize that chronic long-term exposure to high viral load and a higher ratio of MHC I/II in CHB hepatocytes could drive immune evasion via presentation of sub-viral particles^{100,104} or a specific repertoire of antigens to the CD8 T cells, leading to a subdued effector response (Fig. 2I and as proposed in Fig. 6I). In contrast, the increased presence of MHC II-expressing hepatocytes in FC patients (Fig. 5, Fig. S11 and S12) may reflect a decrease in MHC I/II ratio in patients displaying reduced antigen load. This in turn may enable an efficient presentation of an as yet uncharacterized but likely distinct repertoire of viral antigens (including HBs) to the CD4-CTLs, as well as activating CD4-CTLs and adaptive memory NK cells to elicit an additive altered adaptive and innate immune response for long-term viral suppression.^{105,106}

Findings from this study lay the foundation for future studies focused on the functional interrogation of the key immunological events during the process of HBsAg loss. However, the loss of exhausted T cells, gain of innate immune activity (marginated neutrophils; LR-NK cells), and the emergence of effector (PRF1+/GZMA+/TNF/NCR3+) CD4-CTLs during the transition towards viral antigen clearance may serve as novel cell state-based prognostic biomarkers that can guide clinical management of CHB. In addition, findings from our studies may also suggest a therapeutic window of opportunity in patients that display reduced levels of viral antigens and exhaustion markers, for the application of next-generation host-directed therapies, such as therapeutic vaccines, checkpoint inhibitors¹⁰⁷ and immune modulators that can activate the innate and/or an altered adaptive immune response to facilitate the achievement of FC. Finally, this study highlights the need to consider the role and hence therapeutic potential of CD4 T cells in the achievement and/or maintenance of FC, while designing the next generation of immunotherapy modalities to treat patients with CHB.

Affiliations

¹Laboratory of Precision Medicine and Cancer Evolution, Genome Institute of Singapore, Agency for Science, Technology and Research (A*STAR), 60 Biopolis St., #02-01 Genome, Singapore 138672; ²Experimental Drug Development Centre, A*STAR, 10 Biopolis Way, Chromos, Singapore 138670, Singapore; ³Department of Medicine, Yong Loo Lin School of Medicine, National University of Singapore, Singapore; ⁴Institute of Molecular and Cell Biology, A*STAR, 61 Biopolis Drive, Proteos, Singapore, 138673, Singapore; ⁵Bioinformatics Institute, A*STAR, 30 Biopolis Street, Matrix, Singapore 138671, Singapore; ⁶Department of Microbiology and Immunology, Yong Loo Lin School of Medicine, National University of Singapore, Singapore; ⁷Cancer Research Center of Lyon (CRCL), INSERM U1052, CNRS UMR5286, Lyon, France; ⁸Translational Immunology Institute (TII), SingHealth-DukeNUS Academic Medical Centre, Singapore 169856, Singapore;

⁹Department of Medicine, National University Hospital, Singapore; ¹⁰Institute of Biomedical Studies, Baylor University, Waco, TX, USA; ¹¹Parker Institute for Cancer Immunotherapy, San Francisco, CA, USA; ¹²Department of Hepatology, Hôpital Croix-Rousse, Hospices Civils de Lyon, Lyon, France; ¹³University of Lyon Claude Bernard 1 (UCLB1), Lyon, France; ¹⁴Department of Medicine SCIAc and the Italian Institute of Technology (IIT) Center for Life Nanosciences (CLNS), University of Rome La Sapienza, Rome, Italy; ¹⁵Division of Gastroenterology and Hepatology, National University Hospital, National University Health System, Singapore

Abbreviations

APC, antigen-presenting cell; cccDNA, covalently closed circular DNA; CHB, chronic hepatitis B; cNK cell, conventional NK cell; CTLs, cytotoxic T lymphocytes; DACS, disease-associated cell states; DC, dendritic cell; FC, functional cure/functionally cured; HBsAg, HBV surface antigen; IFN, interferon; LR-NK cell, liver-resident NK cell; KC, Kupffer cell; MDSC, myeloid-derived suppressor cell; NK, natural killer; NUC, nucleos(t)ide analogues; PBMC, peripheral blood mononuclear cells; qHBsAg, quantitative HBsAg; scRNA-seq, single-cell RNA sequencing; Tregs, regulatory T cells.

Financial support

This work was supported by Singapore National Medical Research Council's grants NMRC/CIRG/1351/2013, NMRC/CSA-SI/0016/2017, NMRC/CIRG/1479/2017 awarded to S.G.L; NMRC/TCR/14-NUHS/2015, and NMRC/OFLCG19May-0038 grants awarded to J.E.C, G.P, S.G.L, R.D. This work was also supported by CZI Seed Network grant CZIF2019-002429 and NRF-CRP grant CRP26-2021-0005 awarded to R.D.

Conflict of interest

Prof. Seng Gee Lim: Advisory Board: Gilead Sciences, Abbott, Roche, Janssen, GlaxoSmithKline, Grifols, Arbutus; Assembly. Speakers Bureau: Gilead Sciences, Abbott; Educational/research funding: Abbott, Merck Sharpe and Dohme, Gilead. All other authors report no conflicts of interest.

Please refer to the accompanying ICMJE disclosure forms for further details.

Authors' contributions

RD, BCN, AKH and SGL were involved in initial conceptualization and experimental study design of the project. BCN, AKH, SN planned and performed wet lab experiments, with critical help from COO, JWTN, HCY, VBA, RS, NK including single cell and flow cytometry assays, and guidance from RD, JEC, NS. BCN conducted scRNA-seq analysis with RD's supervision. SN, OM, VC performed CytOF analysis. AYLT, MKS, HHTWK, JN, HY, NSBMN, CS, MA, SGL were involved in sample collection. WY, MS, KHO and BCN performed mIF analysis. MLP and ML performed the virology studies using ddPCR. BCN, AKH, NS and RD wrote the manuscript with critical inputs from all authors including SGL and ML.

Data availability statement

All sequencing data has been uploaded to the SRA under BioProject PRJNA1096305 and Study SRP499879 with accessions from SRR28562212-SRR28562261. Metadata for this study can be viewed on the SRA Run Selector at <https://www.ncbi.nlm.nih.gov/Traces/study/?acc=SRP499879>.

Acknowledgements

We would like to thank Prof. Dr. Antonio Bertoletti and Dr. Nina Le Bert, Duke-NUS Medical School, for their critical feedback in improving the manuscript. We would like to thank Dr. Hwee Kuan Lee, BII, A*STAR for his support and guidance. We would like to thank Mr. Samydurai Sudhagar and the Genome Institute of Singapore's S2GP facility (Spatial and Single Cell Platform) for the support. We thank Ms Ming Jie Lim in her assistance to the scRNAseq experiments. We thank Mr. Weiyoung Chua for his administrative support. We thank Ms Xiaoning Wang and NUSMed Flow Cytometry Laboratory Unit for their support. We would like to thank all patients as without their support this study was not possible.

Supplementary data

Supplementary data to this article can be found online at <https://doi.org/10.1016/j.jhep.2024.02.017>.

References

- [1] Aliabadi E, Urbanek-Quaing M, Maasoumy B, et al. Impact of HBsAg and HBcAg levels on phenotype and function of HBV-specific T cells in patients with chronic hepatitis B virus infection. *Gut* 2022 Nov;71(11):2300–2312.
- [2] Choi HSJ, Tonthat A, Janssen HLA, et al. Aiming for functional cure with established and novel therapies for chronic hepatitis B. *Hepatol Commun* 2022 May;6(5):935–949.
- [3] Fung S, Choi HSJ, Gehring A, et al. Getting to HBV cure: the promising paths forward. *Hepatology* 2022 Jul;76(1):233–250.
- [4] Comber M, Lok AS, Terrault NA, et al. Guidance for design and endpoints of clinical trials in chronic hepatitis B - Report from the 2019 EASL-AASLD HBV Treatment Endpoints Conference(double dagger). *J Hepatol* 2020;72:539–557.
- [5] Iannaccone M, Guidotti LG. Immunobiology and pathogenesis of hepatitis B virus infection. *Nat Rev Immunol* 2022;22:19–32.
- [6] Maini MK, Boni C, Lee CK, et al. The role of virus-specific CD8(+) cells in liver damage and viral control during persistent hepatitis B virus infection. *J Exp Med* 2000;191:1269–1280.
- [7] Rivino L, Le Bert N, Gill US, et al. Hepatitis B virus-specific T cells associate with viral control upon nucleos(t)ide-analogue therapy discontinuation. *J Clin Invest* 2018;128:668–681.
- [8] Le Bert N, Gill US, Hong M, et al. Effects of hepatitis B surface antigen on virus-specific and global T cells in patients with chronic hepatitis B virus infection. *Gastroenterology* 2020;159:652–664.
- [9] Dunn C, Brunetto M, Reynolds G, et al. Cytokines induced during chronic hepatitis B virus infection promote a pathway for NK cell-mediated liver damage. *J Exp Med* 2007;204:667–680.
- [10] Gill US, Peppa D, Micco L, et al. Interferon alpha induces sustained changes in NK cell responsiveness to hepatitis B viral load suppression in vivo. *PLoS Pathog* 2016;12:e1005788.
- [11] Chiale C, Marchese AM, Robek MD. Innate immunity and HBV persistence. *Curr Opin Virol* 2021;49:13–20.
- [12] Zimmer CL, Rinker F, Honer Zu Siederdissen C, et al. Increased NK cell function after cessation of long-term nucleos(t)ide analogue treatment in chronic hepatitis B is associated with liver damage and HBsAg loss. *J Infect Dis* 2018;217:1656–1666.
- [13] De Simone G, Andreata F, Bleriot C, et al. Identification of a Kupffer cell subset capable of reverting the T cell dysfunction induced by hepatocellular priming. *Immunity* 2021;54:2089–2100 e2088.
- [14] van Buuren N, Ramirez R, Turner S, et al. Characterization of the liver immune microenvironment in liver biopsies from patients with chronic HBV infection. *JHEP Rep* 2022;4:100388.
- [15] Montanari NR, Ramirez R, Aggarwal A, et al. Multi-parametric analysis of human livers reveals variation in intrahepatic inflammation across phases of chronic hepatitis B infection. *J Hepatol* 2022 Aug;77(2):332–343.
- [16] Genshaft A.S., Subudhi S., Keo A., et al. Clinical implementation of single-cell RNA sequencing using liver fine needle aspirate tissue sampling and centralized processing captures compartment specific immuno-diversity. *bioRxiv* 2021.11.30.470634; doi: <https://doi.org/10.1101/2021.11.30.470634>
- [17] European Association for the Study of the Liver. Electronic address eee, European association for the study of the L. EASL 2017 clinical practice guidelines on the management of hepatitis B virus infection. *J Hepatol* 2017;67:370–398.
- [18] Sharma A, Seow JJW, Dutertre CA, et al. Onco-fetal reprogramming of endothelial cells drives immunosuppressive macrophages in hepatocellular carcinoma. *Cell* 2020;183:377–394 e321.
- [19] Tan AT, Loggi E, Boni C, et al. Host ethnicity and virus genotype shape the hepatitis B virus-specific T-cell repertoire. *J Virol* 2008;82:10986–10997.
- [20] Wolock SL, Lopez R, Klein AM. Scrublet: computational identification of cell doublets in single-cell transcriptomic data. *Cell Syst*. 2019;8:281–291 e289.
- [21] Hao Y, Hao S, Andersen-Nissen E, et al. Integrated analysis of multimodal single-cell data. *Cell* 2021;184:3573–3587 e3529.
- [22] Efremova M, Vento-Tormo M, Teichmann SA, et al. CellPhoneDB: inferring cell-cell communication from combined expression of multi-subunit ligand-receptor complexes. *Nat Protoc* 2020;15:1484–1506.
- [23] La Manno G, Soldatov R, Zeisel A, et al. RNA velocity of single cells. *Nature* 2018;560:494–498.
- [24] MacParland SA, Liu JC, Ma XZ, et al. Single cell RNA sequencing of human liver reveals distinct intrahepatic macrophage populations. *Nat Commun* 2018;9:4383.

Single cell atlas of functionally cured CHB patients

- [25] Zhou Y, Zhou B, Pache L, et al. Metascape provides a biologist-oriented resource for the analysis of systems-level datasets. *Nat Commun* 2019;10:1523.
- [26] Babicki S, Arndt D, Marcu A, et al. Heatmapper: web-enabled heat mapping for all. *Nucleic Acids Res* 2016;44:W147–W153.
- [27] Chew V, Lai L, Pan L, et al. Delineation of an immunosuppressive gradient in hepatocellular carcinoma using high-dimensional proteomic and transcriptomic analyses. *Proc Natl Acad Sci U S A* 2017;114:E5900–E5909.
- [28] Yeo JG, Wasser M, Kumar P, et al. The Extended Polydimensional Immunoome Characterization (EPIC) web-based reference and discovery tool for cytometry data. *Nat Biotechnol* 2020;38:679–684.
- [29] Lebossé F, Inchauspé A, Locatelli M, et al. Quantification and epigenetic evaluation of the residual pool of hepatitis B covalently closed circular DNA in long-term nucleoside analogue-treated patients. *Scientific Rep* 2020;10:21097.
- [30] Styner M, Brechbuhler C, Szekely G, et al. Parametric estimate of intensity inhomogeneities applied to MRI. *IEEE Trans Med Imaging* 2000;19:153–165.
- [31] Bankhead P, Loughey MB, Fernandez JA, et al. QuPath: open source software for digital pathology image analysis. *Sci Rep* 2017;7:16878.
- [32] Rosin PL. Unimodal thresholding. *Pattern Recognit* 2001;34:2083–2096.
- [33] Korsunsky I, Millard N, Fan J, et al. Fast, sensitive and accurate integration of single-cell data with Harmony. *Nat Methods* 2019;16:1289–1296.
- [34] Andrews TS, Atif J, Liu JC, et al. Single-cell, single-nucleus, and spatial RNA sequencing of the human liver identifies cholangiocyte and mesenchymal heterogeneity. *Hepatol Commun* 2022 Apr;6(4):821–840.
- [35] Takeuchi A, Saito T. CD4 CTL, a cytotoxic subset of CD4(+) T cells, their differentiation and function. *Front Immunol* 2017;8:194.
- [36] Sottile R, Panjwani MK, Lau Colleen M, et al. Human cytomegalovirus expands a CD8+ T cell population with loss of BCL11B expression and gain of NK cell identity. *Sci Immunol* 2021;6:eabe6968.
- [37] Correia MP, Cardoso EM, Pereira CF, et al. Hepatocytes and IL-15: a favorable microenvironment for T cell survival and CD8+ T cell differentiation. *J Immunol* 2009;182:6149–6159.
- [38] Correia MP, Costa AV, Uhrberg M, et al. IL-15 induces CD8+ T cells to acquire functional NK receptors capable of modulating cytotoxicity and cytokine secretion. *Immunobiology* 2011;216:604–612.
- [39] Correia MP, Stojanovic A, Wels WS, et al. Innate-like NKp30(+)CD8(+) T cells armed with TCR/CAR target tumor heterogeneity. *Oncoimmunology* 2021;10:1973783.
- [40] Moreno-Nieves UY, Tay JK, Saumyaa S, et al. Landscape of innate lymphoid cells in human head and neck cancer reveals divergent NK cell states in the tumor microenvironment. In: Proceedings of the National Academy of Sciences. 118; 2021, e2101169118.
- [41] Boettler T, Panther E, Bengsch B, et al. Expression of the interleukin-7 receptor alpha chain (CD127) on virus-specific CD8+ T cells identifies functionally and phenotypically defined memory T cells during acute resolving hepatitis B virus infection. *J Virol* 2006;80:3532–3540.
- [42] Radziewicz H, Ibegbu CC, Fernandez ML, et al. Liver-infiltrating lymphocytes in chronic human hepatitis C virus infection display an exhausted phenotype with high levels of PD-1 and low levels of CD127 expression. *J Virol* 2007;81:2545–2553.
- [43] Hoogeveen RC, Dijkstra S, Bartsch LM, et al. Hepatitis B virus-specific CD4 T-cell responses differentiate functional cure from chronic surface antigen+ infection. *J Hepatol* 2022 Nov;77(5):1276–1286.
- [44] Cuff AO, Robertson FP, Stegmann KA, et al. Eomeshi NK cells in human liver are long-lived and do not recirculate but can be replenished from the circulation. *J Immunol* 2016;197:4283–4291.
- [45] Stegmann KA, Robertson F, Hansi N, et al. CXCR6 marks a novel subset of T-bet(lo)Eomes(hi) natural killer cells residing in human liver. *Sci Rep* 2016;6:26157.
- [46] Fisicaro P, Rossi M, Vecchi A, et al. The good and the bad of natural killer cells in virus control: perspective for anti-HBV therapy. *Int J Mol Sci* 2019;20.
- [47] Zhou J, Peng H, Li K, et al. Liver-resident NK cells control antiviral activity of hepatic T cells via the PD-1-PD-L1 Axis. *Immunity* 2019;50:403–417 e404.
- [48] Yuen MF. Biological gradient of chronic hepatitis B. *Nat Rev Gastroenterol Hepatol* 2021;18:593.
- [49] Cao S, Liu M, Sehrawat TS, et al. Regulation and functional roles of chemokines in liver diseases. *Nat Rev Gastroenterol Hepatol* 2021;18:630–647.
- [50] Vilgelm AE, Richmond A. Chemokines modulate immune surveillance in tumorigenesis, metastasis, and response to immunotherapy. *Front Immunol* 2019;10:333.
- [51] Zhou SL, Dai Z, Zhou ZJ, et al. Overexpression of CXCL5 mediates neutrophil infiltration and indicates poor prognosis for hepatocellular carcinoma. *Hepatology* 2012;56:2242–2254.
- [52] De Filippo K, Rankin SM. The secretive life of neutrophils revealed by intravital microscopy. *Front Cell Dev Biol* 2020;8:603230.
- [53] Geh D, Leslie J, Rumney R, et al. Neutrophils as potential therapeutic targets in hepatocellular carcinoma. *Nat Rev Gastroenterol Hepatol* 2022;19:257–273.
- [54] Leslie J, Geh D, Elsharkawy AM, et al. Metabolic dysfunction and cancer in HCV: shared pathways and mutual interactions. *J Hepatol* 2022 Jul;77(1):219–236.
- [55] Doyle NA, Bhagwan SD, Meek BB, et al. Neutrophil margination, sequestration, and emigration in the lungs of L-selectin-deficient mice. *J Clin Invest* 1997;99:526–533.
- [56] Summers C, Rankin SM, Condliffe AM, et al. Neutrophil kinetics in health and disease. *Trends Immunol* 2010;31:318–324.
- [57] Franco A, Barnaba V, Natali P, et al. Expression of class I and class II major histocompatibility complex antigens on human hepatocytes. *Hepatology* 1988;8:449–454.
- [58] Herkel J, Jagemann B, Wiegard C, et al. MHC class II-expressing hepatocytes function as antigen-presenting cells and activate specific CD4 T lymphocytes. *Hepatology* 2003;37:1079–1085.
- [59] Lu JG, Ji P, French SW. The major histocompatibility complex class II-CD4 immunologic synapse in alcoholic hepatitis and autoimmune liver pathology: the role of aberrant major histocompatibility complex class II in hepatocytes. *Am J Pathol* 2020;190:25–32.
- [60] Ghasemi F, Tessier TM, Gameiro SF, et al. High MHC-II expression in Epstein-Barr virus-associated gastric cancers suggests that tumor cells serve an important role in antigen presentation. *Sci Rep* 2020;10:14786.
- [61] Axelrod ML, Cook RS, Johnson DB, Balko JM. Biological consequences of MHC-II expression by tumor cells in cancer. *Clin Cancer Res* 2019;25:2392–2402.
- [62] Gill US, Pallett LJ, Thomas N, et al. Fine needle aspirates comprehensively sample intrahepatic immunity. *Gut* 2019;68:1493–1503.
- [63] Pallett LJ, Gill US, Quaglia A, et al. Metabolic regulation of hepatitis B immunopathology by myeloid-derived suppressor cells. *Nat Med* 2015;21:591–600.
- [64] Gill US, Pallett LJ, Kennedy PTF, et al. Liver sampling: a vital window into HBV pathogenesis on the path to functional cure. *Gut* 2018;67:767–775.
- [65] Park J-J, Wong DK, Wahed AS, et al. Hepatitis B virus-specific and global T-cell dysfunction in chronic hepatitis B. *Gastroenterology* 2016;150:684–695.e685.
- [66] Gang M, Wong P, Berrien-Elliott MM, et al. Memory-like natural killer cells for cancer immunotherapy. *Semin Hematol* 2020;57:185–193.
- [67] Nikzad R, Angelo LS, Aviles-Padilla K, et al. Human natural killer cells mediate adaptive immunity to viral antigens. *Sci Immunol*. 2019;4.
- [68] Paust S, Blish CA, Reeves RK. Redefining memory: building the case for adaptive NK cells. *J Virol* 2017;JVI:169. 00117.
- [69] Paust S, Gill HS, Wang BZ, et al. Critical role for the chemokine receptor CXCR6 in NK cell – mediated antigen-specific memory of haptens and viruses. 11. Nature Publishing Group; 2010. p. 1127–1135.
- [70] Brillantes M, Beaulieu AM. Memory and memory-like NK cell responses to microbial pathogens. *Front Cell Infect Microbiol* 2020;10:102.
- [71] Schuch A, Zecher BF, Muller PA, et al. NK-cell responses are biased towards CD16-mediated effector functions in chronic hepatitis B virus infection. *J Hepatol* 2019;70:351–360.
- [72] Hofmann M, Thimme R. Hepatitis B vaccine and NK cells: a new player in memory. *Gut* 2021;70:229–230.
- [73] Fumagalli V, Venzin V, Di Lucia P, et al. Group 1 ILCs regulate T cell-mediated liver immunopathology by controlling local IL-2 availability. *Sci Immunol*. 2022;7:eaib6112.
- [74] Bihl F, Germain C, Luci C, Braud VM. Mechanisms of NK cell activation: CD4+ T cells enter the scene. *Cell Mol Life Sci* 2011;68:3457.
- [75] Fehniger TA, Cooper MA, Nuovo GJ, et al. CD56bright natural killer cells are present in human lymph nodes and are activated by T cell-derived IL-2: a potential new link between adaptive and innate immunity. *Blood* 2003;101:3052–3057.
- [76] Wu Y, Tian Z, Wei H. Developmental and functional control of natural killer cells by cytokines. *Front Immunol* 2017;8:930.
- [77] He X-S, Draghi M, Mahmood K, et al. T cell-dependent production of IFN-gamma by NK cells in response to influenza A virus. *J Clin Invest* 2004;114:1812–1819.

- [78] Jost S, Tomezsko PJ, Rands K, et al. CD4+ T-cell help enhances NK cell function following therapeutic HIV-1 vaccination. *J Virol* 2014;88:8349–8354.
- [79] McKinstry KK, Alam F, Flores-Malavet V, et al. Memory CD4 T cell-derived IL-2 synergizes with viral infection to exacerbate lung inflammation. *PLoS Pathog* 2019;15:e1007989.
- [80] Buschow SI, Jansen D. CD4(+) T cells in chronic hepatitis B and T cell-directed immunotherapy. *Cells* 2021;10.
- [81] Ben Khelil M, Godet Y, Abdeljaoued S, et al. Harnessing antitumor CD4(+) T cells for cancer immunotherapy. *Cancers (Basel)* 2022;14.
- [82] DeTemple DE, Oldhafer F, Falk CS, et al. Hepatocyte-induced CD4(+) T cell alloresponse is associated with major histocompatibility complex class II up-regulation on hepatocytes and suppressible by regulatory T cells. *Liver Transpl* 2018;24:407–419.
- [83] Mohamadkhani A, Sotoudeh M, Bowden S, et al. Downregulation of HLA class II molecules by G1896A pre-core mutation in chronic hepatitis B virus infection. *Viral Immunol*. 2009;22:295–300.
- [84] Ghosh S, Chakraborty A, Banerjee S. Persistence of hepatitis B virus infection: a multi-faceted player for hepatocarcinogenesis. *Front Microbiol* 2021;12:678537.
- [85] Snell LM, Xu W, Abd-Rabbo D, et al. Dynamic CD4(+) T cell heterogeneity defines subset-specific suppression and PD-L1-blockade-driven functional restoration in chronic infection. *Nat Immunol* 2021;22:1524–1537.
- [86] Wiggins BG, Pallett LJ, Li X, et al. The human liver microenvironment shapes the homing and function of CD4(+) T-cell populations. *Gut* 2022 Jul;71(7):1399–1411.
- [87] Hensel N, Gu Z, Sagar, et al. Memory-like HCV-specific CD8+ T cells retain a molecular scar after cure of chronic HCV infection. *Nat Immunol* 2021;22:229–239.
- [88] Heim K, Binder B, Sagar, et al. TOX defines the degree of CD8+ T cell dysfunction in distinct phases of chronic HBV infection. *Gut* 2021;70: 1550–1560.
- [89] Fisicaro P, Valdatta C, Massari M, et al. Combined blockade of programmed death-1 and activation of CD137 increase responses of human liver T cells against HBV, but not HCV. *Gastroenterology* 2012;143:1576–1585.e1574.
- [90] Barili V, Vecchi A, Rossi M, et al. Unraveling the multifaceted nature of CD8 T cell exhaustion provides the molecular basis for therapeutic T cell reconstitution in chronic hepatitis B and C. *Cells* 2021;10.
- [91] Dienes HP, Hutteroth T, Hess G, et al. Immunolectron microscopic observations on the inflammatory infiltrates and HLA antigens in hepatitis B and non-A, non-B. *Hepatology* 1987;7:1317–1325.
- [92] Schreiber S, Honz M, Mamozi W, et al. Characterization of a library of 20 HBV-specific MHC class II-restricted T cell receptors. *Mol Ther Methods Clin Dev* 2021;23:476–489.
- [93] Koch KS, Leffert HL. Ectopic expression of CD74 in Ikkbeta-deleted mouse hepatocytes. *Acta Histochem* 2011;113:428–435.
- [94] Su H, Na N, Zhang X, Zhao Y. The biological function and significance of CD74 in immune diseases. *Inflamm Res* 2017;66:209–216.
- [95] Tan AT, Hoang LT, Chin D, et al. Reduction of HBV replication prolongs the early immunological response to IFN α therapy. *J Hepatol* 2014;60:54–61.
- [96] Heuberger C, Pott J, Maloy KJ. Why do intestinal epithelial cells express MHC class II? *Immunology* 2021;162:357–367.
- [97] Wosen JE, Mukhopadhyay D, Macaubas C, et al. Epithelial MHC class II expression and its role in antigen presentation in the gastrointestinal and respiratory tracts. *Front Immunol* 2018;9:2144.
- [98] Shenoy AT, Lyon De Ana C, Arafa El, et al. Antigen presentation by lung epithelial cells directs CD4(+) TRM cell function and regulates barrier immunity. *Nat Commun* 2021;12:5834.
- [99] Roche PA, Furuta K. The ins and outs of MHC class II-mediated antigen processing and presentation. *Nat Rev Immunol* 2015;15:203–216.
- [100] Khakpoor A, Ni Y, Chen A, et al. Spatiotemporal differences in presentation of CD8 T cell epitopes during hepatitis B virus infection. *J Virol* 2019;93.
- [101] Gehring AJ, Haniffa M, Kennedy PT, et al. Mobilizing monocytes to cross-present circulating viral antigen in chronic infection. *The J Clin Invest* 2013;123:3766–3776.
- [102] Gehring AJ, Sun D, Kennedy PT, et al. The level of viral antigen presented by hepatocytes influences CD8 T-cell function. *J Virol* 2007;81:2940–2949.
- [103] Diepolder HM, Ries G, Jung M-C, et al. Differential antigen-processing pathways of the hepatitis B virus e and core proteins. *Gastroenterology* 1999;116:650–657.
- [104] Vaillant A. HBsAg, subviral particles, and their clearance in establishing a functional cure of chronic hepatitis B virus infection. *ACS Infect Dis* 2021;7:1351–1368.
- [105] Chen Y, Cheng M, Tian Z. Hepatitis B virus down-regulates expressions of MHC class I molecules on hepatoplasma cell line. *Cell Mol Immunol* 2006;3:373–378.
- [106] Borrego F, Ulbrecht M, Weiss EH, et al. Recognition of human histocompatibility leukocyte antigen (HLA)-E complexed with HLA class I signal sequence-derived peptides by CD94/NKG2 confers protection from natural killer cell-mediated lysis. *J Exp Med* 1998;187:813–818.
- [107] Gane E, Verdon DJ, Brooks AE, et al. Anti-PD-1 blockade with nivolumab with and without therapeutic vaccination for virally suppressed chronic hepatitis B: a pilot study. *J Hepatol* 2019;71:900–907.